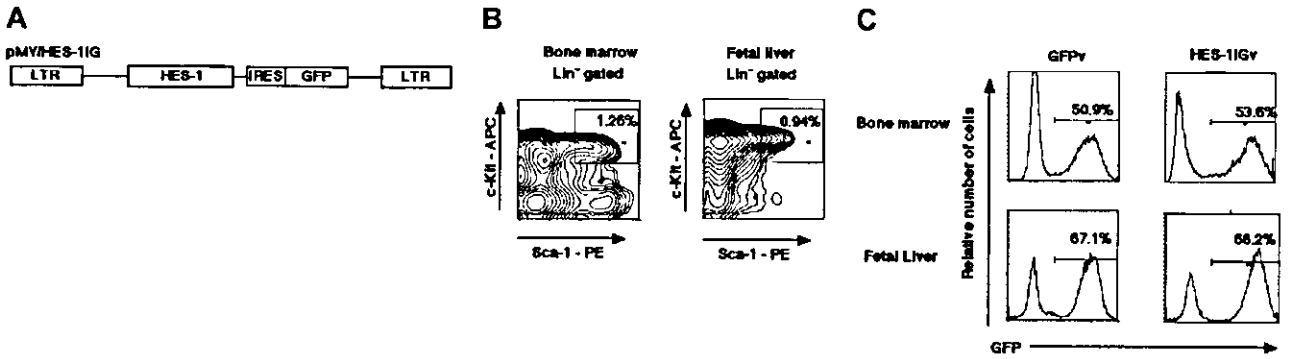

Figure 1. Retroviral construct, stem cells, and transduction. (A) Schematic representation of the retroviral vector, pMY/HES-1IG, encoding HES-1 linked by internal ribosome entry site (IRES) to a cDNA encoding EGFP. (B) Flow cytometric analysis of murine hematopoietic stem cells in adult bone marrow and fetal liver. Staining profile of Sca-1 versus c-Kit on lineage-negative populations in bone marrow (left) and fetal liver (right) cells. (C) Flow cytometric analysis for GFP in infected c-Kit$^+$ Sca-1$^+$ Lin$^-$ (KSL) cells of bone marrow (top) and fetal liver (bottom). Efficiency of infection of these populations is indicated.

particularly when the assay was performed after an additional 3-day culture. The HES-1Igv–transduced L-KSL–derived cells also formed a significantly higher number of HPP-mix–derived colonies than the GFPv-transduced L-KSL–derived cells (Figure 2A). We then transplanted 1000 of the GFP$^+$ B-KSL– and L-KSL–derived cells sorted soon after the 48-hour infection period to sublethally irradiated recipient mice. In both B-KSL– and L-KSL–derived cell transplant recipients, donor cell chimerism was initially established but rapidly decreased within 2 months after transplantation in the control GFPv-transduced group, whereas high levels of chimerism were maintained for up to 6 months after transplantation in the HES-1Igv–transduced group in both myeloid and lymphoid lineages (Figure 2B). Immunophenotyping of the bone marrow, spleen, and thymus cells at 3 months after transplantation confirmed that donor chimerism in these tissues was similar to that in the blood cells (data not shown).

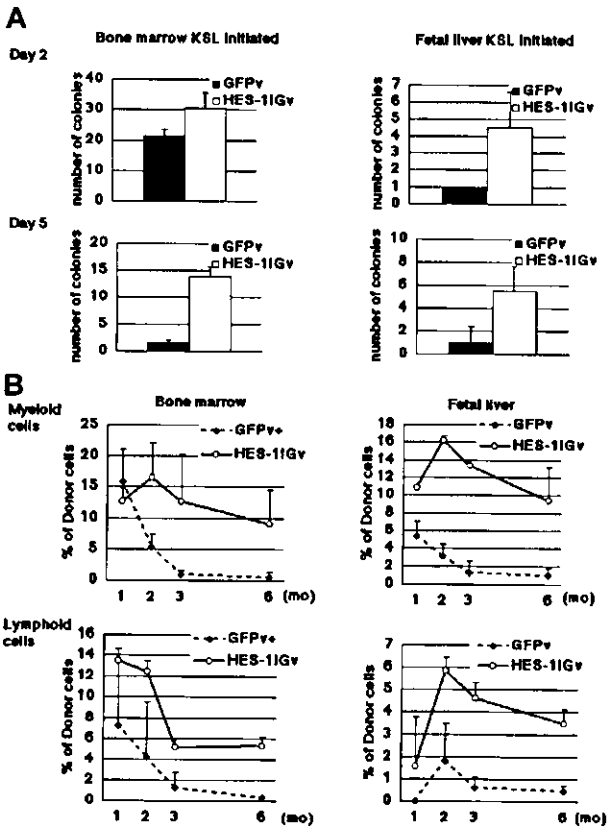

Figure 2. Relative preservation of KSL phenotype by constitutive expression of HES-1. (A) Colony-forming ability of transduced cells was examined soon after sorting GFP$^+$ cells and after an additional 3-day culture. HPP-mix; colonies larger than 1.5 mm in diameter and consisting of at least granulocyte/macrophage and erythroid clusters. The number of HPP-mix–derived colonies in 1000 cells (culture day 2; sort day 0) or 2000 cells (culture day 5; sort day 3) is shown. Data show the mean ± SD of triplicates from 2 independent experiments. (B) Long-term repopulation ability of selected transduced cells was assessed by transplantation to sublethally irradiated recipients. Donor (GFP$^+$Ly5.1$^+$)–derived cells were detected in peripheral blood of recipient mice (Ly5.2). The percentage of donor-derived cells within myeloid (Mac-1$^+$ and Gr-1$^+$) and lymphoid (Thy1.2$^+$ and B220$^+$) cells was measured at various time points after transplantation. Results for HES-1IGv and GFPv are shown as the mean ± SD of 12 and 9 measurements, respectively, from 3 independent experiments (2-6 animals per experiment).

We next examined the ratios of KSL populations in the recipient bone marrow. Recipient-derived (GFP$^-$) and donor-derived (GFP$^+$) bone marrow cells contained similar ratios (0.117% ± 0.054% and 0.092% ± 0.021%, respectively) of KSL in the GFPv-transduced cell transplant group. In contrast, an approximately 5-fold higher ratio (0.577% ± 0.109%) of donor-derived bone marrow cells showed the KSL phenotype in the HES-1Igv–transduced cell transplant group (Figure 3A). In GFP$^+$ KSL sorted from the recipient bone marrow of the GFPv and HES-1IGv groups, RT-PCR confirmed a lower level of *HES-1* mRNA expression in KSL from the GFPv-transduced group and a higher level in KSL from the HES-1Igv–transduced group (Figure 3B).

HES-1 maintains stem cell activity of 34$^-$KSL in vitro

The findings above indicated that HES-1 decreases the rate of loss of immaturity and preserves self-renewability of KSL in vitro. This encouraged us to examine whether HES-1 could maintain 34$^-$KSL cells, the most highly purified HSCs, which have never been shown to be expanded or even maintained in vitro. Although FL has often been used for retrovirus gene transfer directed to HSCs because infection efficiency is generally very low without it, it has been reported that the use of FL is associated with the loss of self-renewal capacity of KSL cells.[37,38] Therefore, we took advantage of omitting FL and used only SCF and TPO for HES-1IGv and GFPv infection of 34$^-$KSL cells (Figure 4A). Both viruses gave an infection efficiency of no less than 20% (Figure 4B). For a competitive LTRA, we also cultured 34$^-$KSL for 48 hours in the same conditions as those for the virus infection, except for the absence of virus. At the end of the 48-hour culture period, most cells lost the 34$^-$KSL phenotype in any virus-transduced and virus-nontransduced group, as anticipated (data not shown). Even KSL cells did not represent a major population in any groups.

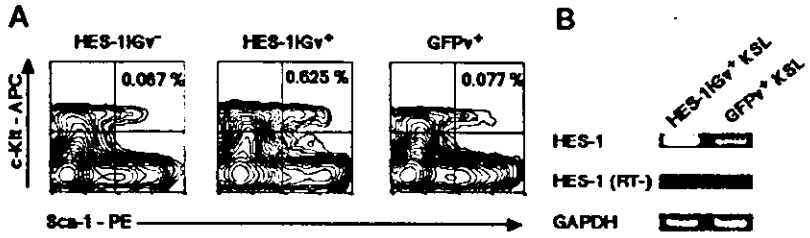

Figure 3. Analysis of bone marrow cells in recipients at 3 months after transplantation. (A) Flow cytometric analysis for KSL in recipient mice. Respective gates for GFP⁻ (recipient-derived, left) and GFP⁺ (donor-derived: HES-1Igv–transduced, middle; GFPv-transduced, right) cells of the lineage-negative population were analyzed for c-Kit and Sca-1 staining. (B) Expression of *HES-1* mRNA in reconstituted cells. The amount of templates for RT-PCR was normalized to give equivalent signals for GAPDH. RT− indicates PCR performed without reverse transcriptase reaction.

Moreover, although the nontransduced 34⁻KSL-derived cells kept the KSL phenotype at 16.7% to 24.9%, GFPv-transduced 34⁻KSL-derived cells kept the KSL phenotype at as low as 8.5% to 13.2%, probably reflecting the fact that only unquiescent and thus differentiation-prone cells are susceptible to retrovirus infection. In contrast, the ratio of KSL in the HES-1Igv–transduced 34⁻KSL-derived cells was 18.6% to 24.7%, which was as high as that in the nontransduced 34⁻KSL-derived cells (Figure 4C).

To better evaluate the effect of HES-1 on 34⁻KSL cells, we performed a competitive LTRA. We transplanted 1000 transduced (GFP⁺-selected, Ly5.1⁺) and the same number of nontransduced 34⁻KSL-derived cells (GFP⁻Ly5.1⁺) to lethally irradiated recipient mice (Ly5.2⁺), and assessed chimerism of the GFP⁺Ly5.1⁺ (tester) and GFP⁻Ly5.1⁺ (competitor) populations in myeloid and lymphoid lineages in the blood at several time points. At all time points examined, the ratios of the tester-derived cells in the total donor-derived cells, that is, the percent of GFP⁺ cells among the Ly5.1⁺ cells, were more than 40% and more than 35% in the myeloid and lymphoid lineages, respectively, in the HES-1Igv–transduced group. In the GFPv-transduced group, in contrast, chimerism of the tester-derived cells in the total donor-derived cells was less than 15% in both lineages at 2 months after the transplantation (Figure 4D). We also assessed GFP⁻Ly5.2⁺ (recipient-derived) cells at each time point and confirmed that this population decreased to a negligible level. These results indicated that stem cell activity of the HES-1Igv–transduced, but not GFPv-transduced, 34⁻KSL-derived cells was almost equivalent to that of the nontransduced 34⁻KSL-derived cells.

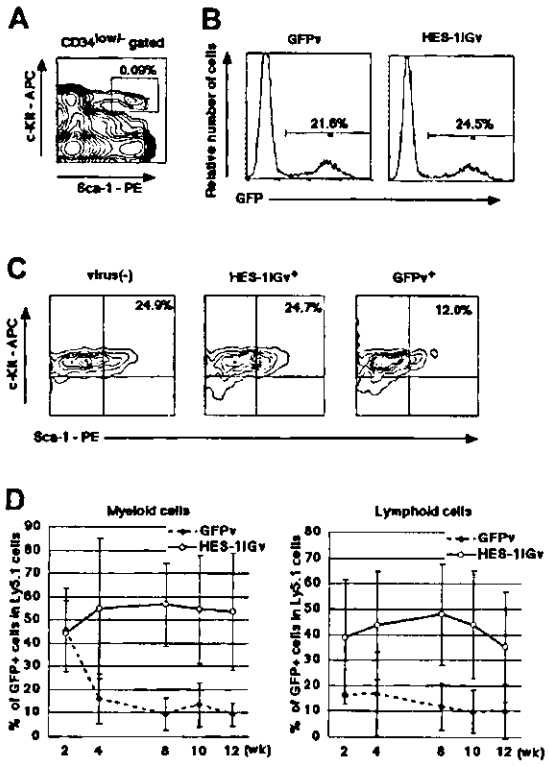

Figure 4. Competitive repopulation assay using 34⁻KSL-derived cells. (A) Staining profile of Sca-1 versus c-Kit in lineage-depleted and CD34$^{-/low}$–gated populations in bone marrow. (B) Flow cytometric analysis for GFP in infected 34⁻KSL-derived cells. Effieciency of infection at the end of the 2-day infection period is indicated. (C) Maintenance of the KSL phenotype in 34⁻KSL-derived cells by HES-1. Left, nontransduced 34⁻KSL-derived cells; middle, HES-1Igv–transduced 34⁻KSL-derived cells; right, GFPv-transduced 34⁻KSL-derived cells. (D) Chimerism of GFP⁺Ly5.1⁺ cells in the total Ly5.1⁺ cells in the blood of recipients. Results for HES-1IGv and GFPv are shown as the mean ± SD of 12 and 8 measurements, respectively, from 3 independent experiments (2 to 6 animals per experiment).

The HES-1⁺ KSL population contains higher ratios of SP and 34$^{low/-}$ cells in the recipient bone marrow and shows higher reconstituting activity

We compared the SP phenotype and CD34 expression profile of the virus-transduced and nontransduced recipient bone marrow KSL in each competitive LTRA recipient mouse. At 3 months after the transplantation, ratios of SP and CD34$^{low/-}$ cells in total KSL were 14.6% and 32.0% in the recipient of the HES-1Igv–transduced 34⁻KSL-derived cell transplant (Figure 5A-B), and 10.7% and 27.3% in the recipient of the GFPv-transduced 34⁻KSL-derived cell transplant (data not shown), respectively. We then separated total KSL into GFP⁻ (mostly virus-nontransduced donor [competitor]–derived) and GFP⁺ (tester-derived) fractions. Remarkably, ratios of SP and CD34$^{low/-}$ cells in the GFP⁺ KSL population were 3.5- and 8-fold higher than those in the GFP⁻ KSL population from the HES-1Igv–transduced cell transplant recipient. In contrast, ratios of SP and CD34$^{low/-}$ cells in the GFP⁺ KSL population were much lower than those in the GFP⁻ KSL population from the GFPv-transduced cell transplant recipient (Figure 5A-B). This indicated that HES-1IGv transduction preserved the KSL cells characterized by the SP and CD34$^{low/-}$ profile, suggesting that HES-1 stores the most immature HSCs without preventing them from supplying mature blood cells.

To further investigate whether the greater ratios of SP and CD34$^{low/-}$ cells in the HES-1⁺ than in the HES-1⁻KSL population truly reflect the greater reconstitution activity of HES-1⁺ than that of HES-1⁻KSL cells, GFP⁺ and GFP⁻ KSL cells were sorted from the bone marrow of HES-1Igv–transduced cell transplant recipients 3 months after the primary transplantation, and 1000 cells from either KSL population were transplanted to lethally irradiated secondary recipient mice (Ly5.2⁺). At 6 months and 10 months after the secondary transplantation, donor chimerism in the blood cells of the secondary recipient was approximately 30% to 40% in the GFP⁺ KSL transplant group and less than 10% in the GFP⁻ KSL transplant group, both in the myeloid and lymphoid lineages (Figure 5C). Although it is more than 1 year since the primary transplantation, no leukemias or lymphomas have developed in any primary or secondary recipient mice (data not shown).

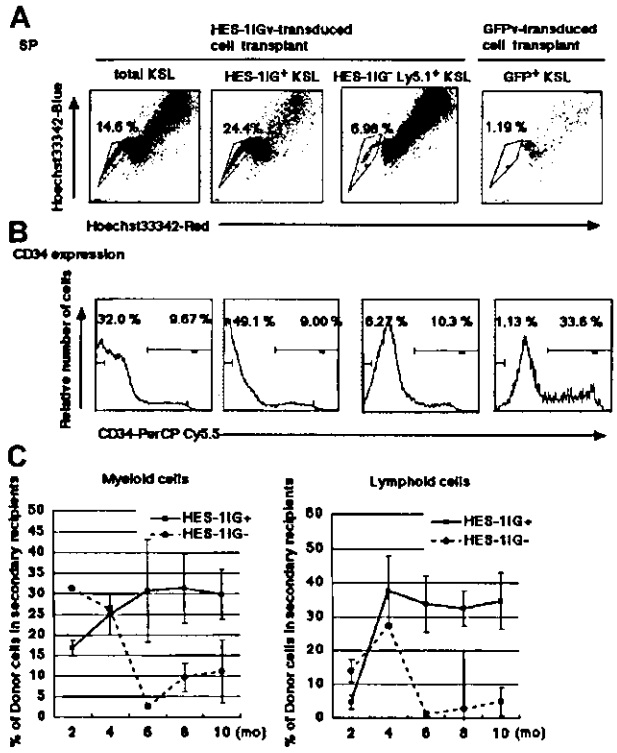

Figure 5. Identification of SP and CD34$^{low/-}$ cells in recipient bone marrow KSL cells. (A) Hoechst dye efflux in various gates of KSL prepared from bone marrow of competitive LTRA recipients. Total KSL, GFP$^+$Ly5.1$^+$ KSL, and GFP$^-$Ly5.1$^+$ KSL from a representative recipient of HES-1Igv–transduced tester cells and competitor cells, and GFP$^+$Ly5.1$^+$ KSL from a representative recipient of GFPv-transduced tester cells and competitor cells were analyzed for staining for Hoechst 33342Blue and Hoechst 33342Red. (B) CD34 expression profile in various gates of KSL prepared from recipients of competitive LTRA. The same gates as panel A were used. To stain CD34 without FITC, PerCP-Cy5.5–labeled mouse CD34 antibody was used. This makes the fluorescence activated cell sorting (FACS) pattern different from that used for CD34$^-$KSL sorting. (C) Evaluation of stem cell activity on secondary transplantation. At each time point, chimerism of donor-derived cells in recipient blood was plotted. Plots are shown as the mean ± SD of 4 animals.

Discussion

In the present study, we demonstrate that retroviral transduction of KSL and 34$^-$KSL with the *HES-1* gene results in preservation of the stem cell activity of these cells in vitro. Moreover, transduction of 34$^-$KSL with *HES-1* results in a striking accumulation of SP and CD34$^{low/-}$ cells among the KSL population in the recipient bone marrow, while maintaining production of differentiated blood cells.

Many investigators have introduced a gene of interest into bone marrow and fetal liver cells by a retroviral gene transfer method and transplanted the transduced cells to recipient animals.[39,40] These studies have described a number of interesting phenotypes in the blood compartment of recipients, such as those showing the development of leukemia and an increase or decrease in hematopoiesis in a certain lineage, and aided understanding of the roles of introduced genes in HSCs. However, with rare exceptions, the use of highly purified HSCs for virus transduction is rare and it has therefore been unclear which cells are transduced. Strictly, none of the previous studies have directly proved the expansion or maintenance of virus-transduced HSCs. A few reports[22,41] have shown multilineage hematolymphopoietic reconstitution in the recipient mice with a sorted single HSC characterized by Lin$^-$, Sca-1$^+$, c-Kit$^+$, and CD34$^{low/-}$. Although 34$^-$KSL cells do not represent a homogenous population, they are the most highly purified HSCs, at least in steady-state adult bone marrow. The use of this population as a target of gene transduction and transplantation to recipient mice greatly facilitates study of the function of the gene of interest and the technology of ex vivo HSC expansion. Normally, culturing purified HSCs for only 48 hours without stromal cells significantly reduces their stem cell activity. Moreover, retrovirus transduction requires cell division, which in general indicates a further decrease in stem cell activity.[37] Given these factors, the decreased ability of GFPv-transduced 34$^-$KSL-derived cells to retain the immature phenotype in vitro and decreased engraftment capacity in mice receiving these cells compared with the nontransduced 34$^-$KSL-derived cells (Figure 4C-D) is reasonable. In clear contrast, these capacities in HES-1Igv–transduced 34$^-$KSL-derived cells are at least the same as those of nontransduced 34$^-$KSL-derived cells (Figure 4C-D), indicating that *HES-1* introduction in 34$^-$KSL cells strongly preserves the original biologic phenotype of these cells in vitro.

HES-1 is a basic helix-loop-helix transcription factor, which functions as a negative regulator for cell differentiation in various systems, such as neurogenesis,[24,42,43] myogenesis,[25,29] and hair cell formation,[44] although it also induces cell differentiation in selected contexts, such as in glial cell differentiation.[33] Down-regulation and up-regulation of HES-1, together with HES-5, in neuronal stem cells in developing mice indicate that this gene functions as a positive regulator of neuronal stem cell self-renewal.[28] Our observation suggests that HES-1 has a similar effect on hematopoietic stem cells.

In addition to its strong ex vivo maintenance capacity for 34$^-$KSL, we showed that HES-1 dramatically accumulates SP and CD34$^{low/-}$ cells in the recipient bone marrow KSL cells. The ability to escape Hoechst dye staining is considered to represent an important feature common to stem cells of various lineages.[32] In the hematopoietic compartment, it has been shown that long-term reconstituting cells exist in SP and that SP and 34$^-$KSL partially overlap.[45] We indeed show that the HES-1$^+$ KSL population that contains a greater ratio of SP and CD34$^{low/-}$ cells has a reconstitution capacity greater than the HES-1$^-$KSL population (Figure 5C). This implies that HES-1 confers an increased self-renewal capacity to the most primitive HSCs in vivo, and we propose that HES-1 is a positive regulator of the expansion of HSCs without exhausting their stem cell activity. The mechanism by which HSC-containing populations such as SP and 34$^-$KSL accumulate while normal differentiation and supply of blood cells are maintained remains to be elucidated.

Recently, phenotypes of the recipients who received transplants of lineage-negative bone marrow cells introduced with HES-1 and HES-5, as well as active Notch-1, were reported.[46] The phenotype of *HES-1*–transduced lineage-negative cell transplant recipients described in that report was similar to ours in that the recipients do not develop T-cell leukemia, in contrast to the fact that T-cell leukemia develops in active Notch-1–transduced lineage-negative cell transplant recipients.[46,47] The finding in the previous report that the recipients had a greater number of clonogenic cells in bone marrow could be similar to our finding that immature clonogenic cells were maintained in vitro or that the recipients had a greater number of stem cells such as SP cells in bone marrow. However, there is a significant difference in the development of lymphoid cells in the recipients. In contrast to the results described in the previous report, we did not find any distortion in the lymphoid compartment of the *HES-1*–transduced HSC transplant recipients. This difference could be attributed to the difference in the experimental system. We used highly purified HSCs for retroviral

gene transfer, implying that we transplanted much fewer numbers of *HES-1*–transduced committed progenitor cells. If less-purified bone marrow cells are used for retroviral transduction, it might be the case that the gene of interest is preferentially introduced into the committed progenitors such as T-cell progenitors, rather than into stem cells, and that in such cases the phenotype derived from progenitors rather than stem cells is prominent.

Interestingly, HES-1 is a direct target of a transcriptional activator complex comprising RBPJ and activated Notch in neurogenic, myogenic, and lymphoid cells. Further, a growing body of evidence shows that activation of Notch signaling results in prevention of differentiation. We therefore expect that if ligands for Notch can efficiently up-regulate HES-1 expression in 34$^-$KSL, they may serve as potential tools for ex vivo HSC expansion, particularly given that ligand-induced up-regulation of HES-1 does not require retrovirus transduction, an experimental system used in this work which is nevertheless disadvantageous to the maintenance of stem cell activity because of requirement of cell division. Indeed, others have already investigated the possibility of Notch ligands for this purpose.[17,18,20] Although these efforts have yet to show clinical impact, our data strongly support their value and the potential for further methodologic development.

In the present study we show using several independent experimental designs that purified HSCs can be maintained ex vivo by HES-1 up-regulation. With technical improvement, the use of Notch ligands or other methods to up-regulate HES-1 carries strong promise for future clinical use.

Acknowledgments

We thank Y. Koyama of Becton Dickinson Hongo Laboratory for assistance in SP analysis. We also thank T. Kitamura for the pMY/IRES-EGFP retrovirus vector, T. Yoshimatsu for the ψMP34 cells, and G. Harris for review of the manuscript.

References

1. Till JE. Proliferation and differentiation of stem cells of the blood-forming system of the mouse. NASA CR-673. NASA Contract Rep NASA CR. 1967:69-75.
2. Tsuji T, Itoh K, Nishimura-Morita Y, et al. CD34high+ CD38(low/-) cells generated in a xenogenic coculture system are capable of both long-term hematopoiesis and multiple differentiation. Leukemia. 1999;13:1409-1419.
3. Nishikawa M, Tahara T, Hinohara A, Miyajima A, Nakahata T, Shimosaka A. Role of the microenvironment of the embryonic aorta-gonad-mesonephros region in hematopoiesis. Ann N Y Acad Sci. 2001;938:109-116.
4. Nolta JA, Thiemann FT, Arakawa-Hoyt J, et al. The AFT024 stromal cell line supports long-term ex vivo maintenance of engrafting multipotent human hematopoietic progenitors. Leukemia. 2002;16:352-361.
5. Matsunaga T, Kato T, Miyazaki H, Ogawa M. Thrombopoietin promotes the survival of murine hematopoietic long-term reconstituting cells: comparison with the effects of FLT3/FLK-2 ligand and interleukin-6. Blood. 1998;92:452-461.
6. Berger M, Fagioli F, Piacibello W, et al. Role of different medium and growth factors on placental blood stem cell expansion: an in vitro and in vivo study. Bone Marrow Transplant. 2002;29:443-448.
7. Shah AJ, Smogorzewska EM, Hannum C, Crooks GM. Flt3 ligand induces proliferation of quiescent human bone marrow CD34+CD38- cells and maintains progenitor cells in vitro. Blood. 1996; 87:3563-3570.
8. Sui X, Tsuji K, Ebihara Y, et al. Soluble interleukin-6 (IL-6) receptor with IL-6 stimulates megakaryopoiesis from human CD34(+) cells through glycoprotein (gp)130 signaling. Blood. 1999;93: 2525-2532.
9. Murray LJ, Young JC, Osborne LJ, Luens KM, Scollay R, Hill BL. Thrombopoietin, flt3, and kit ligands together suppress apoptosis of human mobilized CD34+ cells and recruit primitive CD34+ Thy-1+ cells into rapid division. Exp Hematol. 1999;27:1019-1028.
10. Weinmaster G, Roberts VJ, Lemke G. A homolog of Drosophila Notch expressed during mammalian development. Development. 1991;113:199-205.
11. Ellisen LW, Bird J, West DC, et al. TAN-1, the human homolog of the Drosophila notch gene, is broken by chromosomal translocations in T lymphoblastic neoplasms. Cell. 1991;66:649-661.
12. Del Amo FF, Smith DE, Swiatek PJ, et al. Expression pattern of Motch, a mouse homolog of Drosophila Notch, suggests an important role in early postimplantation mouse development. Development. 1992;115:737-744.
13. Weinmaster G, Roberts VJ, Lemke G. Notch2: a second mammalian Notch gene. Development. 1992;116:931-941.
14. Artavanis-Tsakonas S, Rand MD, Lake RJ. Notch signaling: cell fate control and signal integration in development. Science. 1999;284:770-776.
15. Shimizu K, Chiba S, Saito T, Kumano K, Hirai H. Physical interaction of Delta1, Jagged1, and Jagged2 with Notch1 and Notch3 receptors. Biochem Biophys Res Commun. 2000;276:385-389.
16. Milner LA, Kopan R, Martin DI, Bernstein ID. A human homologue of the Drosophila developmental gene, Notch, is expressed in CD34+ hematopoietic precursors. Blood. 1994;83:2057-2062.
17. Varnum-Finney B, Purton LE, Yu M, et al. The Notch ligand, Jagged-1, influences the development of primitive hematopoietic precursor cells. Blood. 1998;91:4084-4091.
18. Jones P, May G, Healy L, et al. Stromal expression of Jagged 1 promotes colony formation by fetal hematopoietic progenitor cells. Blood. 1998; 92:1505-1511.
19. Kaneta M, Osawa M, Sudo K, Nakauchi H, Farr AG, Takahama Y. A role for pref-1 and HES-1 in thymocyte development. J Immunol. 2000;164: 256-264.
20. Karanu FN, Murdoch B, Gallacher L, et al. The notch ligand jagged-1 represents a novel growth factor of human hematopoietic stem cells. J Exp Med. 2000;192:1365-1372.
21. Varnum-Finney B, Xu L, Brashem-Stein C, et al. Pluripotent, cytokine-dependent, hematopoietic stem cells are immortalized by constitutive Notch1 signaling. Nat Med. 2000;6:1278-1281.
22. Osawa M, Hanada K, Hamada H, Nakauchi H. Long-term lymphohematopoietic reconstitution by a single CD34-low/negative hematopoietic stem cell. Science. 1996;273:242-245.
23. Sasai Y, Kageyama R, Tagawa Y, Shigemoto R, Nakanishi S. Two mammalian helix-loop-helix factors structurally related to Drosophila hairy and enhancer of split. Genes Dev. 1992;6:2620-2634.
24. Ishibashi M, Ang SL, Shiota K, Nakanishi S, Kageyama R, Guillemot F. Targeted disruption of mammalian hairy and enhancer of split homolog-1 (HES-1) leads to up-regulation of neural helix-loop-helix factors, premature neurogenesis, and severe neural tube defects. Genes Dev. 1995;9:3136-3148.
25. Jarriault S, Brou C, Logeat F, Schroeter EH, Kopan R, Israel A. Signalling downstream of activated mammalian Notch. Nature. 1995;377:355-358.
26. Jarriault S, Le Bail O, Hirsinger E, et al. Delta-1 activation of notch-1 signaling results in HES-1 transactivation. Mol Cell Biol. 1998;18:7423-7431.
27. Tomita K, Hattori M, Nakamura E, Nakanishi S, Minato N, Kageyama R. The bHLH gene Hes1 is essential for expansion of early T cell precursors. Genes Dev. 1999;13:1203-1210.
28. Ohtsuka T, Sakamoto M, Guillemot F, Kageyama R. Roles of the basic helix-loop-helix genes Hes1 and Hes5 in expansion of neural stem cells of the developing brain. J Biol Chem. 2001;276:30467-30474.
29. Shawber C, Nofziger D, Hsieh JJ, et al. Notch signaling inhibits muscle cell differentiation through a CBF1-independent pathway. Development. 1996;122:3765-3773.
30. Goodell MA, Brose K, Paradis G, Conner AS, Mulligan RC. Isolation and functional properties of murine hematopoietic stem cells that are replicating in vivo. J Exp Med. 1996;183:1797-1806.
31. Goodell MA, Rosenzweig M, Kim H, et al. Dye efflux studies suggest that hematopoietic stem cells expressing low or undetectable levels of CD34 antigen exist in multiple species. Nat Med. 1997;3:1337-1345.
32. Zhou S, Schuetz JD, Bunting KD, et al. The ABC transporter Bcrp1/ABCG2 is expressed in a wide variety of stem cells and is a molecular determinant of the side-population phenotype. Nat Med. 2001;7:1028-1034.
33. Ishibashi M, Moriyoshi K, Sasai Y, Shiota K, Nakanishi S, Kageyama R. Persistent expression of helix-loop-helix factor HES-1 prevents mammalian neural differentiation in the central nervous system. Embo J. 1994;13:1799-1805.
34. Yoshimatsu T, Tamura M, Kuriyama S, Ikenaka K. Improvement of retroviral packaging cell lines by introducing the polyomavirus early region. Hum Gene Ther. 1998;9:161-172.
35. Onishi M, Nosaka T, Misawa K, et al. Identification and characterization of a constitutively active STAT5 mutant that promotes cell proliferation. Mol Cell Biol. 1998;18:3871-3879.
36. Kagami S, Nakajima H, Suto A, et al. Stat5a regulates T helper cell differentiation by several distinct mechanisms. Blood. 2001;97:2358-2365.
37. Ema H, Takano H, Sudo K, Nakauchi H. In vitro

self-renewal division of hematopoietic stem cells. J Exp Med. 2000;192:1281-1288.

38. Adolfsson J, Borge OJ, Bryder D, et al. Upregulation of Flt3 expression within the bone marrow Lin(-)Sca1(+)c-kit(+) stem cell compartment is accompanied by loss of self-renewal capacity. Immunity. 2001;15:659-669.
39. Thorsteinsdottir U, Sauvageau G, Humphries RK. Enhanced in vivo regenerative potential of HOXB4-transduced hematopoietic stem cells with regulation of their pool size. Blood. 1999;94: 2605-2612.
40. Izon DJ, Punt JA, Xu L, et al. Notch1 regulates maturation of CD4+ and CD8+ thymocytes by modulating TCR signal strength. Immunity. 2001; 14:253-264.
41. Sato T, Laver JH, Ogawa M. Reversible expression of CD34 by murine hematopoietic stem cells. Blood. 1999;94:2548-2554.
42. Kageyama R, Sasai Y, Akazawa C, et al. Regulation of mammalian neural development by helix-loop-helix transcription factors. Crit Rev Neurobiol. 1995;9:177-188.
43. Cau E, Gradwohl G, Casarosa S, Kageyama R, Guillemot F. Hes genes regulate sequential stages of neurogenesis in the olfactory epithelium. Development. 2000;127:2323-2332.
44. Zheng JL, Shou J, Guillemot F, Kageyama R, Gao WQ. Hes1 is a negative regulator of inner ear hair cell differentiation. Development. 2000; 127:4551-4560.
45. Bunting KD. ABC transporters as phenotypic markers and functional regulators of stem cells. Stem Cells. 2002;20:11-20.
46. Kawamata S, Du C, Li K, Lavau C. Overexpression of the Notch target genes Hes in vivo induces lymphoid and myeloid alterations. Oncogene. 2002;21:3855-3863.
47. Allman D, Karnell FG, Punt JA, et al. Separation of Notch1 promoted lineage commitment and expansion/transformation in developing T cells. J Exp Med. 2001;194:99-106.

Molecular characterization of the recurrent unbalanced translocation der(1;7)(q10;p10)

Lili Wang, Seishi Ogawa, Akira Hangaishi, Ying Qiao, Noriko Hosoya, Yasuhito Nanya, Kazuma Ohyashiki, Hideaki Mizoguchi, and Hisamaru Hirai

An unbalanced translocation der(1;7)(q10;p10) is a nonrandom chromosomal aberration commonly observed in myelodysplastic syndrome and acute myeloid leukemia. We molecularly analyzed the breakpoints of der(1;7)(q10;p10) by quantitative fluorescent in situ hybridization (FISH) analyses using centromeric satellite DNAs mapped to chromosomes 1 and 7 as probes. We found that the signal intensities of 2 centromere alphoid probes, D1Z7 on chromosome 1 and D7Z1 on chromosome 7, were almost invariably reduced on the derivative chromosome compared with those on their normal counterparts. These results suggest that this translocation results from the recombination between the 2 alphoids, which was further confirmed by fiber FISH experiments. Because the relative reduction in the intensities of D1Z7 and D7Z1 signals on the derivative chromosomes was highly variable among patients, it was estimated that the breakpoints in these patients were randomly distributed over several megabase pairs within each alphoid cluster except for its extreme end to the short arm. Our results provide a novel insight into the structural basis for generation of this translocation as well as its leukemogenic roles. (Blood. 2003;102: 2597-2604)

Introduction

The unbalanced whole-arm translocation of chromosome 1 (chr1) and chromosome 7 (chr7), der(1;7)(q10;p10), is a nonrandom chromosomal abnormality first described by Geraedts et al.[1] It is commonly found in myelodysplastic syndrome (MDS) and acute myeloid leukemia (AML) and less frequently in myeloproliferative disorders, involving all subgroups of MDS and AML. Since more than half of the patients had a history of previous antitumor chemotherapy (especially containing alkylating agents) and/or radiotherapy or occupational exposure to toxic agents, it has been causally related to secondary or therapy-related MDS or AML.[2-9] In MDS, as many as 6% of the patients are reported to have this karyotypic abnormality. They typically present trilineage morphologic myelodysplasia in the bone marrow and pancytopenia in the peripheral blood and have a high rate of progression to AML with generally poor prognosis.[10,11]

This unbalanced translocation, typically described as 46, XY (or XX), +1, der(1;7)(q10;p10), has 2 prominent cytogenetic characteristics: (1) it retains only 1 of 2 possible derivative chromosomes, containing 1q and 7p; and (2) there are 2 copies of apparently normal chr1 and only 1 copy of normal chr7, resulting in trisomy of 1q and monosomy of 7q (Figure 1). In the early fluorescent in situ hybridization (FISH) studies, several authors pointed out the dicentric nature of this translocation, in a sense that the signals of the 2 alphoids from chr1 and chr7 are colocalized on the derivative chromosome. Alitalo et al[12] reported that FISH signals of D1Z5 and D7Z2 coexisted on the der(1;7)(q10;p10), and others[13,14] also described that D1Z5 and D7Z1 cohybridized to the derivative chromosome in this translocation. However, no further molecular analysis, especially concerning exact locations of the breakpoints and their distribution, has been conducted to date.

In this paper, in order to disclose the genomic mechanism generating der(1;7)(q10;p10), we focused on the centromere alphoid sequences on chr1 and chr7 and dissected the structural alterations associated with this translocation by the 2-color FISH method with simultaneous measurements of FISH signals.

Patients, materials, and methods

Clinical samples

A total of 27 bone marrow samples were collected from patients carrying der(1;7)(q10;p10) and subjected to FISH analysis. The patients' profiles are summarized in Table 1. All patients gave their informed consent to the sample collection and to the biologic analyses included in the present study according to the Declaration of Helsinki. Giemsa trypsin G-banding (GTG-banding) analysis was performed according to the standard protocol.[15]

DNA probes

The screening of bacterial artificial chromosome (BAC) or P1-based artificial chromosome (PAC) clones was previously described.[16] DNA from BACs or PACs was extracted using the Large-Construct Kit (QIAGEN, Tokyo, Japan). A D1Z7 clone, pE25.a, was purchased from American Type Culture Collection (ATCC; Manassas, VA). A clone of D7Z1, called D7Z1^{6mer}, was obtained from polymerase chain reaction (PCR) amplification with primers spanning the dimer and the tetramer of the published

From the Department of Hematology and Oncology, Graduate School of Medicine, University of Tokyo, Japan; the First Department of Internal Medicine, Tokyo Medical University, Japan; and the Department of Hematology, Tokyo Women's Medical University, Japan.

Submitted January 6, 2003; accepted June 5, 2003. Prepublished online as *Blood* First Edition Paper, June 19, 2003; DOI 10.1182/blood-2003-01-0031.

Supported in part by Grant-In-Aid for Scientific Research (KAKENHI 13307029).

Reprints: Hisamaru Hirai, Department of Hematology & Oncology, Graduate School of Medicine, University of Tokyo 7-3-1 Hongo, Bunkyo-ku, Tokyo 113-8655, Japan; e-mail: hhirai-tky@umin.ac.jp.

The publication costs of this article were defrayed in part by page charge payment. Therefore, and solely to indicate this fact, this article is hereby marked "advertisement" in accordance with 18 U.S.C. section 1734.

Figure 1. Partial karyotype of der (1;7)(q10;p10). GTG-banding analysis from Pt 1 shows that the whole long arm of chromosome 1 (chr1) and the whole short arm of chromosome 7 (chr7) fuse to constitute der(1;7)(q10;p10) (der).

D7Z1 sequences (National Center for Biotechnology Information [NCBI] accession: M16087, M16101). The sequences of the primers were 5′-TCCACTTGCAAATTCCACAA-3′ and 5′-TGGATATATGGACCG-CATTG-3′. The probes of satellite III (SatIII) and D7Z2 were also generated by PCR. Primers for SatIII (GenBank database X60726) were 5′-TCCATTCCAGTCCATTCGAT-3′ and 5′-AATCATCATCCAACG-GAAGC-3′ and those for D7Z2 (NCBI accession: G31642) were 5′-CTGGAGGCGGATATTAGGGT-3′ and 5′-CTGGGAATACTTCTGTC-TAT-3′. All the plasmid DNAs were extracted using QIAGEN Plasmid Maxi Kit (QIAGEN). Three directly labeled probes, CEP 1/5 (Spectrum Orange), CEP 1 (Spectrum Orange), and CEP 7 (Spectrum Green), which detect the sequences of D1Z7, D1Z5, and D7Z1, respectively, were purchased from VYSIS (Downers Grove, IL).

FISH analysis

FISH experiments on metaphase chromosomes and interphase nuclei were performed as described[17] with some modifications in posthybridization washes, which consisted of 2 × standard saline citrate (SSC)/50% formamide at 37°C for 15 minutes followed by 2 × SSC and 1 × SSC at room temperature for 15 minutes each. Biotin- and digoxigenin-labeled probes were detected with avidin–fluorescein isothiocyanate (FITC; Roche, Mannheim, Germany) and anti–digoxigenin-rhodamine Fab fragments (Roche), respectively. For fiber FISH experiments, the released chromatin fibers were prepared as described[18] and hybridized with 2 directly labeled probes, CEP 1/5 and CEP 7, following the procedures recommended by the manufacturer. Samples were examined with a Nikon E800 epi-fluorescence microscope (Tokyo, Japan) at × 1000 magnification, and the FISH images were captured to 8-bit–depth image files using a Kodak KAF1400 thermoelectronically cooled charge-coupled device (CCD) camera (Roper Scientific, Tucson, AZ) and the SimpleVision software (Digital Scientific, Cambridge, United Kingdom) through a triple–band-pass filter, which allowed rhodamine, FITC, and DAPI (4,6 diamidino-2-phenylindole) signals to be captured without any image displacement. For each experiment, more than 30 metaphase images taken under exact focus conditions were stored. The whole intensity of each signal was automatically computed as the sum of pixel intensities under the indicated area by using the IP lab/PathVysion Extras software (Scanalytics, Fairfax, VA), and finally the average was taken from the 30 measurements together with calculation of the standard deviation. The allelic origin of the 7p and 1q components of the der(1;7)(q10;p10) was determined by comparing the signal intensity of polymorphic satellite elements on chr1 (SatIII) and on chr7 (D7Z2), which were safely apart from the breakpoints and their sequences were expected to be completely reserved on the der(1;7)(q10;p10) in tumor cells.

Southern blot analysis

Neo1 and An4, Neo7 and NT18, Neo2, Neo16, and Neo19, were monochromosomal human-mouse hybrid cell lines containing human chromosome 1, 7, 2, 16, and 19, respectively, and were purchased from the JCRB Cell Bank (Japanese Collection of Research Bioresources, Osaka, Japan). Genomic DNAs were extracted from the cell lines[19] and subjected to Southern blot analysis essentially as described.[20] High-stringency hybridization was done at 53°C for 16 to 18 hours in hybridization solution containing 50%

Table 1. Cytogenetic profile of patients

Patient	Age, y/sex	Diagnosis	Karyotype
1	45/M	MDS (RA)	46,XY,+1,der(1;7)(q10;p10),add(10)(q?)[20]
2	74/M	MDS (RA)	46,XY,+1,der(1;7)(q10;p10)[18]
3	67/M	MDS (RA)	46,XY,+1,der(1;7)(q10;p10)[9]/46,XY[6]
4	74/M	MDS (RA)	46,XY,+1,der(1;7)(q10;p10),del(20)(q11)[12]/45,idem,−20[4]
5	66/M	MDS, MF	46,XY,+1,der(1;7)(q10;p10)[5]/47,idem,+8[13]
6*	58/M	MDS (RA)	46,XY,+1,der(1;7)(q10;p10)[3]/46,XY[18]
7*	53/F	MDS	46,XX,+1,der(1;7)(q10;p10)[12]/46,X,−X,+1,der(1;7)(q10;p10),+der(1;7)(q10;p10), −2,+5,+6,−8,−12,+14,−16,−17,+18,+21[1]/46,XX[7]
8*	70/M	MDS (RA)	46,XY,+1,der(1;7)(q10;p10)[18]/46,XY[2]
9*	67/M	MDS (RA)	46,XY,+1,der(1;7)(q10;p10)[1]/47,idem,+8⅔/46,idem,del(20)(q11)[2]/47,idem,+8,del(20)(q11)[15]
10	51/M	MDS (RAEB)	46,XY,+1,der(1;7)(q10;p10)[19]/45,X,−Y,idem[1]
11	53/M	MDS	46,XY,+1,der(1;7)(q10;p10)[20]
12	68/M	MDS	46,XY,+1,der(1;7)(q10;p10)[10]/46,XY[10]
13	49/M	MDS (RA)	46,XY,+1,der(1;7)(q10;p10)[12]/46,XY[8]
14	49/M	AML (M0)	46,XY,+1,der(1;7)(q10;p10)[20]
15*	68/M	AML (M2)	46,XY,+1,der(1;7)(q10;p10)[5]/47,idem,+8[16]
16	88/M	MDS (RA)	47,XY,+1,der(1;7)(q10;p10),del(20)(q?),del(20)[9]/46,XY[10]
17	56/M	MDS (RA)	46,XY,+1,der(1;7)(q10;p10)[18]/46,XY[4]
18*	47/M	MF	46,XY,+1,der(1;7)(q10;p10)[16]/46,XY[2]
19	58/M	MDS (RA)	46,XY,+1,der(1;7)(q10;p10)[3]/47,idem,+8[16]/46,XY[2]
20*	74/M	MDS (RA)	46,XY,+1,der(1;7)(q10;p10)[13]/46,XY[1]
21*	68/M	MDS (RAEB-t)	46,XY,+1,der(1;7)(q10;p10)[14]/46,XY[6]
22	54/M	MDS (RA)	46,XY,+1,der(1;7)(q10;p10)[2]/46,XY[18]
23	72/M	MF	46,XY,+1,der(1;7)(q10;p10)[1]/46,XY,del(13)(q10q21)[4]/46,XY[14]
24*	57/M	MM	46,XY,+1,der(1;7)(q10;p10)[5]/46,XY[16]
25*	70/M	MDS (RA)	46,XY,+1,der(1;7)(q10;p10)[9]
26	72/M	AML (M0)	46,XY,+1,der(1;7)(q10;p10)[17]/45,idem,−14[1]/45,idem,−21[1]/46,XY[1]
27	58/M	MDS/AML	47,XY,+1,der(1;7)(q10;p10),+8[4]/47,idem,del(20)(q11)[1]/46,XY[1]

RA indicates refractory anemia; MF, myelofibrosis; RAEB, refractory anemia with excess blasts; M0, minimally differentiated acute myeloblastic leukemia; M2, acute myeloblastic leukemia with maturation; RAEB-t, refractory anemia with excess blasts in transformation; and MM, multiple myeloma.

*Therapy-related cases.

formamide, 5 × SSC, and 1 × Denhaldt solution. The final wash was performed at 65°C in 0.1 × SSC/0.1% sodium dodecyl sulfate (SDS) for 20 minutes.

Results

Breakpoint mapping of der(1;7)(q10;p10) by FISH

Initially, in order to map the breakpoint of der(1;7)(q10;p10), we repeatedly performed FISH experiments using a series of probes already mapped to, or newly isolated from, the pericentric regions of chr1 and chr7. Finally, the breakpoints were mapped between D1Z1 and D1S3445 on chr1 and between D7Z2 and sWSS295 on chr7, when no more BAC probes could be obtained to extend the contigs because of a heavy load of repetitive sequences around these regions (data not shown). It was noted, however, that the FISH signals of D1Z7 (probe pE25.a) on the derivative chromosome always looked weaker compared with those on normal chr1s in most cases, raising a possibility that the breakpoints on chr1 might be within the D1Z7 alphoid region. On the other hand, several BAC clones mapped to the pericentromeric region of chr7 seemed to produce a reduced FISH signal on the derivative chromosome when compared with the signal on the normal chr7 in tumor cells. Subsequent database analyses and Southern blot experiments revealed that these BAC clones characteristically had varying contents of D7Z1 alphoid sequences (data not shown), suggesting that the breakpoint on chr7 might be associated with the D7Z1 alphoid cluster.

Identification of the allelic chr1 and chr7 counterparts of the derivative chromosome

Both D1Z7 and D7Z1 belong to the centromere alpha satellite DNAs (or alphoid DNA), which are characterized by a large block of tandem repeats (a subset) spanning from 250 kilobase (kb) to 5000 kb, depending on chromosomes.[19,21-24] Each alphoid subset is composed of highly ordered repeats of multimers, which consist of homologous 171–base pair (bp) monomer units. According to their sequence homology and array structure, alphoid subsets can be divided into 5 different suprachromosomal families.[21] Because alphoid DNAs typically show extensive polymorphism regarding the number of their tandem repeats,[25-27] we had to determine the exact allelic origin of the derivative chromosome before properly evaluating the reduction of the D1Z7 and D7Z1 signals on this chromosome, as the intensity of these FISH signals directly depends on their cluster length.

To this end, we used the other 2 repetitive sequences as the allelic references, SatIII on 1q11 to q12[21,28,29] and D7Z2 on the short-arm side of D7Z1 on chr7,[30,31] which also exhibit a prominent allelic polymorphism. When FISH was performed using D1Z7 and SatIII probes, as shown in Figure 2A-F and 2M, the origins of the 2 homologous chr1s could be distinguished by the relative intensity of their SatIII signals, which were uniform among all the metaphases from normal as well as abnormal (tumor) cells (Table 2), indicating that the 2 apparently normal chr1s in tumor cells have different allelic origins and did not result from duplication of either of the 2. Of note is that the SatIII signal on the derivative chromosome always had the same intensity as either of the 2 SatIII signals on the normal chr1s. Similarly, using D7Z2 probes, relative intensities of the 2 D7Z2 signals in abnormal and, if existed, normal metaphases were also uniform (Figure 2G-L,O; Table 3), showing that the short-arm portion of the derivative chromosome and the remaining normal chr7 had different allelic origins. Given

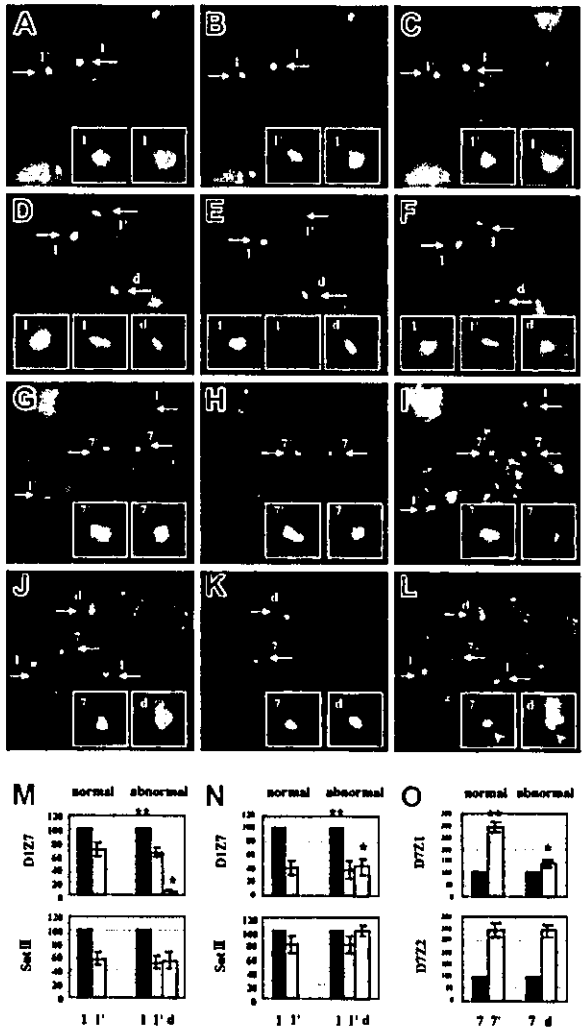

Figure 2. Representative results of 2-color FISH experiments and comparison of signal intensities in centromere alphoids. Two-color FISH was performed with SatIII (green) and D1Z7 (red) probes for normal (A-C) and abnormal (D-F) metaphases in Pt 6 and with D7Z2 (red), 97G24 (red), and D7Z1 (green) probes for normal (G-I) and abnormal (J-L) metaphases in Pt 16. 97G24 is a PAC probe located on 1q13 that helps detect trisomy of 1q. Images for FITC (B,E,H,K), Rhodamin (C,F,I,L), and both (A,D,G,J) were separately captured through a single triple–band-pass filter with an appropriate first-pass filter using a synchronized wheel filter device. 1 and 1′, 7 and 7′, and d indicate different alleles of chr1, chr7, and derivative chromosome, respectively. Captured images were subjected to measurement of signal intensities. Original magnification, × 1000. Intensity of the D1Z7 signal on derivative chromosome (*) is grossly reduced from its original intensity (**), as determined using SatIII intensity as a reference in Pt 6 (M) and Pt 8 (N). Likewise, D7Z1 signal on derivative chromosome (*) is also shown to decrease when compared with its original signal (**), as determined using D7Z2 intensity in Pt 16 (O). Arrows in panels A-L indicate the centromeres of chromosome 1, chromosome 7, or the derivative chromosome. Arrowheads in panel L point to the D7Z2 signals in order to distinguish these signals from the red signals of 97G24. Error bars represent the SD from 30 measurements in 1 patient.

these measurements, we could determine the origins of chr1 and chr7 portions of the derivative chromosome using SatIII and D7Z2 as allelic markers, respectively, and thus quantitatively evaluate the alteration of the signal intensities on the derivative chromosome on an allelic basis.

Reduction of the D1Z7 and D7Z1 signal intensities on the derivative chromosome

Comparison of the D1Z7 signals based on the SatIII marker showed that the signal intensity of D1Z7 on the derivative chromosome was clearly reduced from that of the normal counterpart to the varying extent in all but one (patient [Pt] 27) of the 27

Table 2. Relative intensities of D1Z7 and SatIII signals on the derivative chromosome and its allelic equivalent

	D1Z7			SatIII		
	Normal cells	Tumor cells		Normal cells	Tumor cells	
Patient	chr1*	chr1*	der	chr1*	chr1*	der
1	ND	124.9 (18.5)	3.8 (2.6)	ND	166.6 (64.2)	168.2 (59.5)
2	ND	80.8 (9.5)	17.5 (5.5)	ND	50.2 (17.4)	48.9 (11.5)
3	190.0 (27.3)	188.3 (24.5)	37.9 (10.7)	57.9 (8.8)	57.2 (10.8)	56.0 (10.3)
4	ND	127.7 (17.6)	15.9 (7.9)	ND	41.3 (8.7)	41.8 (10.2)
5	ND	128.0 (19.1)	7.0 (4.7)	ND	68.7 (13.3)	68.3 (12.6)
6	68.5 (9.2)	64.3 (7.8)	5.7 (3.3)	56.3 (9.0)	51.5 (8.4)	53.7 (11.4)
7	163.4 (24.5)	158.2 (39.0)	28.8 (14.7)	46.7 (5.3)	45.9 (9.2)	46.1 (7.6)
8	225.5 (46.9)	233.8 (57.2)	104.9 (37.0)	129.9 (23.4)	131.9 (25.4)	130.1 (22.0)
9	ND	75.6 (8.3)	43.5 (7.0)	ND	65.0 (4.8)	69.0 (6.3)
10	ND	191.6 (41.2)	31.3 (12.9)	ND	48.1 (6.6)	48.9 (7.7)
11	ND	64.3 (9.6)	37.4 (8.9)	ND	266.5 (59)	265.6 (52.2)
12	124.7 (14.8)	122.2 (14.5)	15.6 (4.2)	52.3 (6.5)	49.5 (6.5)	49.0 (8.7)
13	152.6 (15.8)	149.2 (12.4)	51.7 (9.3)	171.5 (24.4)	174.1 (30.6)	176.1 (30.5)
14	ND	140.2 (13.1)	50.7 (7.7)	ND	21.2 (4.6)	19.3 (7.1)
15	ND	149.5 (13.3)	56.6 (9.7)	ND	269.3 (43.3)	270.1 (38.0)
16	78.2 (6.1)	78.1 (8.4)	33.3 (8.3)	167.5 (11.6)	169.3 (18.5)	170.4 (18.1)
17	130.8 (9.5)	129.2 (9.8)	8.4 (2.7)	75.2 (6.5)	72.1 (7.1)	72.1 (6.8)
18	ND	70.7 (7.1)	10.2 (7.0)	ND	63.2 (8.2)	63.2 (8.0)
19	ND	149.7 (14.9)	24.8 (6.6)	ND	60.9 (10.3)	62.1 (9.8)
20	64.7 (9.1)	65.3 (6.5)	33.4 (3.7)	45.3 (7.0)	43.4 (6.5)	43.1 (8.4)
21	153.6 (8.7)	158.5 (18.1)	69.1 (10.0)	51.7 (4.2)	50.8 (10.0)	50.8 (9.3)
22	149.4 (10.8)	143.4 (19.0)	31.3 (12.6)	20.8 (2.8)	21.7 (3.6)	20.6 (4.7)
23	185.0 (10.7)	179.0 (17.5)	45.3 (13.9)	138.9 (6.5)	137.1 (13.1)	136.7 (17.1)
24	137.4 (6.1)	142.8 (13.0)	58.5 (14.2)	34.9 (2.8)	35.2 (4.4)	35.8 (6.3)
25	ND	160.5 (16.0)	51.6 (7.9)	ND	52.9 (7.5)	52.6 (6.6)
26	ND	192.9 (8.7)	22.7 (6.0)	ND	22.0 (1.8)	22.7 (2.7)
27	52.9 (4.9)	53.8 (5.5)	0	45.7 (3.1)	45.1 (6.1)	47.4 (6.2)

The allelic equivalent of the derivative chromosome for chr1 was determined by comparing the relative intensities of SatIII signals within normal and abnormal metaphases. Then the intensities of D1Z7 and SatIII on the derivative chromosome and its equivalent normal chr1 were expressed as relative values to those on their homologous chr1, where the latter were set to 100. The mean values calculated from 30 measurements for normal and abnormal metaphases are presented, and the standard deviations are given in parentheses.

der indicates the derivative chromosome; and chr1*, the normal chr1 from which the derivative chromosome was generated. ND indicates that there is either no detectable normal metaphase in the samples or that the normal metaphases are too little to get a reliable statistical estimation.

samples examined (the ratios of D1Z7 and SatIII signals are summarized in Table 2). Even when the D1Z7 signal on one of the normal chr1s seemed weaker than that on the derivative chromosome, the signal reduction in the latter could also be detected when compared properly with its authentic normal counterpart (Figure 2N). In the same manner the reduction of the D7Z1 signal on the derivative chromosome was also demonstrated, except for Pt 27, using D7Z2 as an allelic reference, though the comparison was more complicated and, in principle, only possible for those samples that contain normal metaphases (Table 3). These observations strongly suggest that the breakpoints of der(1;7)(q10:p10) are located within the D1Z7 alphoid cluster on chr1 and D7Z1 on chr7.

FISH analysis of D1Z5 alphoid clusters

D1Z5 is another kind of alphoid on the centromere of chr1 and is clustered on both sides of the D1Z7 alphoid.[17,32] Results from interphase FISH and fiber FISH experiments suggest that there seems to be no intervening sequences between these alphoids.[17] When the interphase nuclei from normal samples were hybridized with a D1Z5 probe (CEP1), the 2 separate clusters of D1Z5 could be clearly recognized as a pair of doublet signals with different signal intensities (Figure 3A). In contrast, in all other tumor samples except for Pt 27, in addition to the 2 pairs of the doublet signals corresponding to the 2 normal chr1s, there was another signal having the intensity comparable to that of the larger signal in one of the 2 doublets (Figure 3B). This indicated that the smaller D1Z5 cluster was lost on the derivative chromosome and that the breakpoint of der(1;7)(q10.p10) exists between the 2 D1Z5 clusters, most likely within the D1Z7 cluster.

Breakpoint in Pt 27

Pt 27 was considered an exceptional case because no visible D1Z7 or D1Z5 signal was detected on the derivative chromosome, whereas the D7Z1 and SatIII signals seemed completely preserved (Tables 2-3; data not shown). This suggested that, in this particular case, the breakpoint should be mapped between the larger cluster of D1Z5 and SatIII on chr1 and between D7Z1 and the 7q tail on chr7 (Figure 4A).

Interphase and fiber FISH analysis

As expected from these results, pE25.a (D1Z7) and D7Z1^{6mer} (D7Z1) signals were observed largely overlapped on metaphase chromosomes as well as in interphase nuclei of der(1;7)(q10;p10) samples in dual-color FISH experiments (Figure 3C-D). To improve the FISH resolution and to further confirm the direct recombination between D1Z7 and D7Z1 in der(1;7)(q10;p10), we performed fiber FISH analysis. As shown in Figure 3E, the D1Z7 (the red beads) and the D7Z1 (the green beads) signals were found directly connected on the same DNA fiber in 10 tumor samples examined (Pt 2-Pt 9, Pt 12, and Pt 20).

Table 3. Relative intensities of D7Z1 and D7Z2 signals on the derivative chromosome and its allelic equivalent

Patient	D7Z1		D7Z2	
	norm	der	norm	der
3	130.2 (11.3)	72.2 (9.1)	283.0 (40.4)	277.5 (38.5)
6	303.7 (9.2)	182.4 (19.3)	69.7 (8.3)	72.1 (8.2)
7	133.0 (14.7)	46.4 (8.4)	49.5 (6.9)	51.8 (7.5)
8	115.0 (11.1)	88.6 (5.9)	48.0 (15.1)	48.6 (9.3)
12	80.2 (9.0)	55.4 (8.7)	364.5 (74.8)	364.2 (70.4)
13	222.6 (16.6)	168.8 (16.5)	245.1 (23.0)	254.3 (29.2)
16	293.3 (25.1)	144.6 (8.3)	293.0 (30.3)	290.3 (25.0)
17	231.4 (22.0)	210.2 (8.6)	233.0 (19.4)	246.1 (16.0)
20	220.7 (15.3)	133.3 (4.0)	64.4 (4.0)	62.8 (2.0)
21	225.5 (18.9)	103.1 (12.3)	177.0 (8.7)	173.1 (14.8)
22	76.3 (4.0)	61.8 (1.6)	181.9 (16.9)	182.3 (9.7)
23	246.8 (22.1)	118.7 (6.7)	55.2 (4.3)	54.8 (5.5)
24	144.2 (5.1)	84.1 (4.0)	74.3 (3.8)	75.5 (2.0)
27	50.1 (4.6)	49.3 (4.7)	172.3 (19.8)	179.6 (27.8)

The allelic equivalent of the derivative chromosome for chr7 was determined by comparing the relative intensities of D7Z2 signals within normal and abnormal metaphases. Then the intensities of D7Z1 and D7Z2 on the derivative chromosome and its equivalent normal chr7 were expressed as relative values to those on their homologous chr7, where the latter were set to 100. The mean values calculated from 30 measurements for normal and abnormal metaphases are presented, and the standard deviations are given in parentheses. We were able to obtain the information regarding the signal reduction of D7Z1 from only 14 of the 27 patients because in the remaining cases, there were either no normal metaphases in their samples or the numbers of normal metaphase were too small to make a reliable statistical assessment.

der indicates the derivative chromosome; and norm, the normal chr7 from which the derivative chromosome was generated.

Distribution of the breakpoints within the alphoid regions

To investigate the characteristics of this translocation more in detail, we focused on the residual proportions of D1Z7 and D7Z1 signals on the derivative chromosome, which could provide a gross estimation for the relative locations of the breakpoints within each cluster. As summarized in Figure 5, the relative reduction in D1Z7 and D7Z1 sequences on the derivative chromosome was different from patient to patient. Considering each alphoid cluster is estimated to be several megabase pairs in length, our results suggest that the breakpoints on chr1 and chr7 are not clustered but widely distributed within the D1Z7 and D7Z1 sequences among these patients.

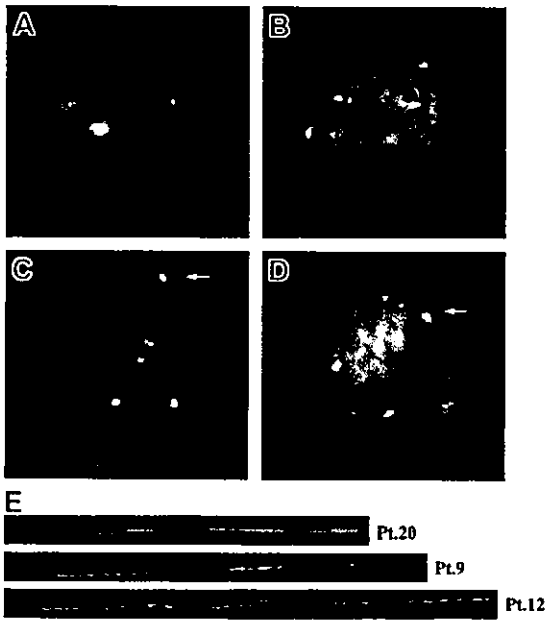

Figure 3. FISH analysis with the patients using various centromeric alphoid probes. Interphase FISH with a D1Z5 probe, CEP1, in normal (A) and abnormal (B) cells. Two-color FISH with pE25.a (green) and D7Z1^{6mer} (red) with tumor cells, showing almost completely overlapped signals (arrows) on metaphase (C) and interphase (D) nuclei. Original magnification, × 1000. (E) Fiber FISH analysis of der(1;7)(q10;p10) using a D1Z7 probe, CEP1/5 (red), and a D7Z1 probe, CEP7 (green), visualizing direct connection of both alphoids on the same DNA fiber.

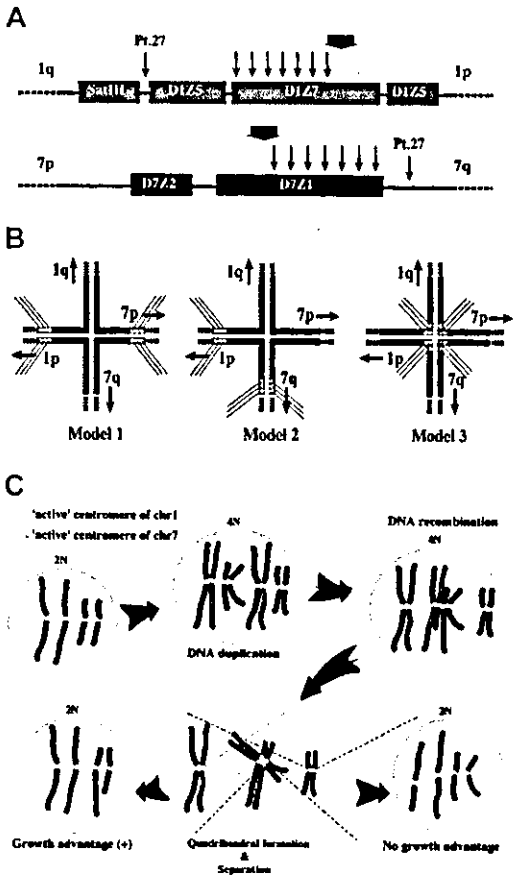

Figure 4. Breakpoint mapping in der(1;7)(q10;p10) and proposed mechanism generating this translocation. (A) Breakpoints are widely distributed within D1Z7 and D7Z1. The ends to the short arm within both alphoids (*) are free from recombinations. A broad arrow indicates the hypothetical critical point on each alphoid. A recombination that occurs beyond this point might compromise segregation of recombined chromosomes and eventually result in their loss. Thin arrows represent the locations of the breakpoints; yellow stars indicate the hypothetic active centromere. (B) Three possible models for the quadriheadral formation with relation to relative location of active centromeres to the breakpoint. Active centromeres may be either contralaterally (Model 1), ipsilaterally (Model 2), or centrally (Model 3) positioned. For the sake of stable maintenance of sister chromatids, the contralateral model might be favored, and only this seems to be compatible with the real distribution of the breakpoints and with allelic distribution in this unbalanced translocation. (C) Proposed mechanism of generation of 46, XY (or XX), +1, der(1;7)(q10;p10). Active centromere sequences on chr1 and chr7 are indicated as yellow and blue circles, respectively. For simplicity, some features of chromosomes are not always as they really are. For example, sister chromatids are depicted separately from before recombination, which should be tightly paired and stuck to each other through cohesion molecules.

Similarity of the 2 involved alphoid subsets

When hybridized to the human genomic DNA at high stringency, D1Z7 (pE25.a) and D7Z1 (D7Z1^{6mer}) produced almost an identical hybridization pattern (Figure 6A). To separately evaluate the specific hybridization of each probe to different homologous alphoids on different human chromosomes, the DNAs from a series of monochromosomal human-mouse hybrid cells were examined

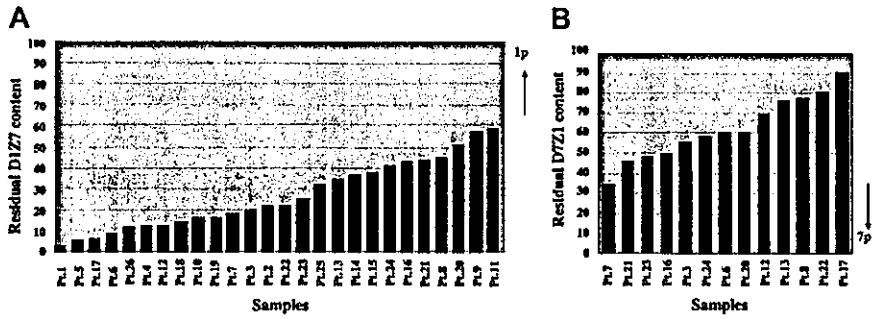

Figure 5. Relative reduction of D1Z7 and D7Z1 contents on the derivative chromosome in different samples. The remaining proportions of D1Z7 (A) and D7Z1 (B) alphoids are depicted based on the measurements of FISH signals. They show great variations from patient to patient, indicating the wide distribution of the breakpoints within each alphoid in der(1;7)(q10;p10). Note that the extreme ends to the short arm within both alphoids are retained, and therefore are devoid of breakpoints. As indicated by the arrows, the 1p portion of D1Z7 and the 7q portion of D7Z1 are lost on the derivative chromosome.

by Southern blot analysis using both probes. Under the same stringent condition, D1Z7 probe strongly hybridized to chr1 but also, to a lesser extent, to chr7, creating the similar hybridization pattern with 3 major bands of 340-bp dimer, 680-bp tetramer, and 1020-bp hexamer (Figure 6B). D7Z1 also created the similar hybridization pattern with stronger hybridization to chr7 than to chr1. While chr16 and chr19 contain alphoids of the same suprachromosomal family 1 as D1Z7 and D7Z1,[20] the hybridization patterns in chr16 and chr19 were substantially different. No hybridization was detected in chr2, which has no suprachromosomal family 1 alphoid. These results indicated that D1Z7 and D7Z1 were more similar than other alphoids of suprachromosomal family 1, not only in their sequence contents but also in their higher-order array structures.

Discussion

On exploring the centromeric fusion in this unbalanced translocation, the conventional methods for identification of chromosomal breakpoints, such as Southern blot analysis, were not available due to the highly repetitive and polymorphic features of the pericentric sequences. Nevertheless, it was these features that allowed us the other approach to molecularly delineate the structure of der(1;7)(q10;p10); variations of the large cluster lengths of the involved alphoid sequences can be easily detected and compared on an allelic basis by measuring the intensity of polymorphic satellite signals. The reproducibility of our signal measurements was satisfactory enough to get a reliable estimation on the alterations of the signal intensity. Although the relationship between the intensity of FISH signals and the alphoid length might not be linear, it was still expected to be monotonic. Given this monotonic relationship, we could grossly estimate the relative reduction in the length of both involved alphoid clusters. According to this estimation, the proportion of shortening of each alphoid sequence is highly variable, indicating that the breakpoints of der(1;7)(q10;p10) translocation were widely distributed within D1Z7 on chr1 and D7Z1 on chr7, although they seemed to spare the extreme end to the short arm within both alphoids (Figure 5). Therefore, it seems unlikely that there exists a unique gene target at or near those breakpoints, and the leukemogenic potential of this translocation may well be ascribed to altered gene dosages resulting from trisomy 1q and/or monosomy 7q, well-known chromosomal abnormalities found in MDS/AML (7q−) as well as many solid cancers (+1q), even though the critical gene targets for these deletion and duplication remain to be unveiled.

FISH analysis in this study also provided additional information as to the structure of the alphoids on chr1, their order being 1p-D1Z5 (smaller cluster)-D1Z7-D1Z5 (larger cluster)-1q. Of interest is that this translocation generates a derivative chromosome that contains 4 alphoid subsets at its centromeric region, 2 from chr1 and the other 2 from chr7 (mapped as 7p-D7Z2-partial D7Z1-partial D1Z7-the larger cluster of D1Z5-1q). This is the first report in the literature that 4 alphoid subsets coexist on a single centromere. Further investigations will be required to understand how this multi-alphoid centromere can function and be maintained in eukaryotic cells.

With regard to the exact sequences that participate in this centromeric fusion, our fiber FISH results strongly indicated that D1Z7 and D7Z1 were directly involved in the DNA recombination. This is also supported by the fact that the centromere alphoid clusters are highly ordered tandem arrays without interruptions by other elements[19,32,33] except at their marginal regions of the cluster.[34,35] In addition, both alphoids have extremely high structural homology, which is estimated to be about 90% at a unit component level. Both are composed of dimer and tetramer repeat units, each of which is defined by *Eco*RI sites. This extreme similarity in their higher-order array structures was also confirmed by our Southern blot experiment (Figure 6). These particular similarities in the unit component as well as higher-order structures seem to make both alphoids especially prone to be recombined to each other.

Although the exact mechanism through which this alphoid recombination takes place is still unclear, we may postulate that it is mediated by an error that occurred during DNA repair processes because, clinically, der(1;7)(q10;p10) has been closely associated with secondary MDS/AML that arises after heavy doses of chemotherapy, especially of alkylating agents, the well-known antitumor drugs that cause DNA double-strand breaks (DSBs).[36,37] As the excessive accumulation of DSBs imposed on either D1Z7 or

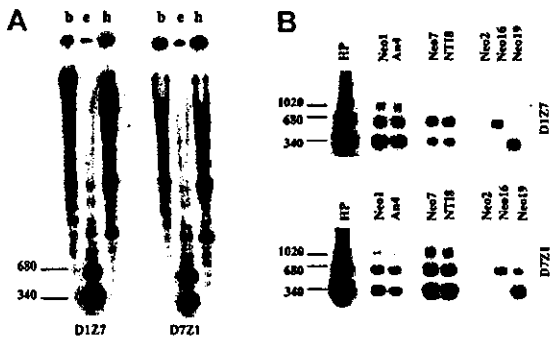

Figure 6. Similarity of the 2 involved alphoid subsets. Southern blot analysis of D1Z7 (pE25.a) and D7Z1 (D7Z1^{6mer}) alphoids in total human genome (A) digested with *Bam*HI (b), *Eco*RI (e), and *Hin*dIII (h), as well as in DNAs from human monochromosomal mouse hybrid cells containing chromosome 1 (Neo1 and An4), 7 (Neo7 and NTI8), 2 (Neo2), 16 (Neo16), or 19 (Neo19) digested with *Eco*RI (B). Locations of dimmer (340 bp), tetramer (680 bp), and hexamer (1020 bp) are indicated to the left. D1Z7 and D7Z1 created a similar hybridization pattern with some cross hybridization with each other.

D7Z1, cells would recruit the repair processes, which are thought to erroneously mediate recombination between these highly homologous alphoid sequences. Given that the initiating DSBs occur randomly, it might be expected that the chromosome having a larger centromere alphoid content would be involved more frequently. In fact, in our case series, the der(1;7) tended to be originated from the homologous chromosome with a larger alphoid content. Participation of the chromosome allele with a larger amount of D1Z7 and D7Z1 was observed in 19 of 26 and 11 of 13 samples, respectively.

From a cytogenetic point of view, der(1;7)(q10;p10) has a consistent feature in that it contains 2 apparently normal chr1s and only one copy of normal chr7, and our analysis has clearly demonstrated that the 2 apparently normal chr1s as well as the remaining chr7 and the 7p of the derivative chromosome in the tumor cells always have different allelic origins. To explain this prominent cytogenetic feature we could assume that the recombination occurs during or after DNA synthesis (Figure 4). In this model, a double-stranded DNA breakage taking place on one of the just-duplicated daughter chromatids of chr1 or chr7 evokes a recombination repair process, during which an error occurs to misconnect the D1Z7 and D7Z1 sequences and leads to the quadriradial formation involving the 2 pairs of daughter chromatids (Figure 4B-C). At this stage, there may be several possibilities as to the way of kinetocore formation and separation of duplicated chromatids, as shown in Figure 4B. This process (mitosis) is thought to involve a number of well-coordinated interactions of DNA and proteins, and, for the time being, we could not know its exact mechanism. However, the cytogenetic profile of the der(1;7)(q10;p10) seems to be most simply explained by Model 1 shown in Figure 4B, in which "active" or "critical" centers of kinetocore formation on the replicated chr1 and chr7 are both polarized to the short arm of each chromosome. According to this model, the quadriradial daughter chromatids, also previously proposed by Morrison-DeLap et al,[5] will be separated following the usual mechanism of mitosis. Of the 2 possible ways of chromatid distributions only one will result in the unbalanced translocation with uneven distribution of chromosomal materials, which might confer a growth advantage to the cells that inherit der(1;7)(q10;p10) (Figure 4C). Although in the budding yeast, only a 125-bp sequence ensures the complete centromere functions including kinetocore attachment, spindle formation, and successful chromatid separation, little has been known about the essential part of mammalian centromeres. In order to explain the unique karyotypic feature of der(1;7)(q10;p10), we hypothesize existence of the sequences related to this active centromere function and kinetocore formation to the centromere region polarized to the short arm of each chromosome. There is no definite evidence for this hypothesis but there are some rationales: first of all, this gives us the simplest explanation. Once the quadriradial structure is formed, the cytogenetic configuration of der(1;7)(q10;p10) under interest will be directly generated without involvement of any other abnormalities in mitotic machinery. Second, our model also holds true for Pt 27, an exceptional case in terms of the location of the breakpoints, because the quadriradial chromatids (Figure 4A-B, Model 1) in Pt 27 are expected to retain the whole of the D7Z1 and D7Z2 clusters on its 7p arm and the whole of the D1Z7 and D1Z5 clusters on its 1p arm. In this case we could more safely conclude that the active centromeres are localized to the 7p and 1p arms. Finally, as shown in Figure 5, the breakpoints strangely spare the short-arm ends of both D1Z7 and D7Z1, where we presumed the hypothetical active centromere elements are localized.

In conclusion, we disclosed the molecular characteristics of der(1;7)(q10;p10), one of the most common forms of chromosomal abnormalities found in secondary MDS/AML. It directly involves 2 centromere alphoids of its participating chromosomes, and the underlying mechanism that gives rise to this translocation seems to be closely related to the structural similarities of both alphoids and their association with centromere functions. It requires further investigation of human centromere structure and its functions to fully understand the entire pathogenesis, which may serve as prevention of this translocation with poor prognosis.

Acknowledgment

We are grateful to Dr Huntington F. Willard for providing us the chromosome 7 alpha satellite probes that were used to confirm the results in our paper.

References

1. Geraedts JP, den Ottolander GJ, Ploem JE, Muntinghe OG. An identical translocation between chromosome 1 and 7 in three patients with myelofibrosis and myeloid metaplasia. Br J Haematol. 1980;44:569-575.
2. Pedersen-Bjergaard J, Philip P, Mortensen BT, et al. Acute nonlymphocytic leukemia, preleukemia, and acute myeloproliferative syndrome secondary to treatment of other malignant diseases: clinical and cytogenetic characteristics and results of in vitro culture of bone marrow and HLA typing. Blood. 1981;57:712-723.
3. Mecucci C, Ghione F, Tricot G, Van den Berghe H. Combined trisomy 1q and monosomy 7q due to translocation 1;7 in myelodysplastic syndromes. Cancer Genet Cytogenet. 1985;18:193-197.
4. Scheres JM, Hustinx TW, Geraedts JP, Leeksma CH, Meltzer PS. Translocation 1;7 in hematologic disorders: a brief review of 22 cases. Cancer Genet Cytogenet. 1985;18:207-213.
5. Morrison-DeLap SJ, Kuffel DG, Dewald GW, Letendre L. Unbalanced 1;7 translocation and therapy-induced hematologic disorders: a possible relationship. Am J Hematol. 1986;21:39-47.
6. Sheppard DM, Richkind KE, Bull M. Translocation 1;7 in four cases of myeloid disorders. Cancer Genet Cytogenet. 1989;38:49-52.
7. Yokoo H, Okada Y, Tominaga K, et al. der(1;7)(q10;p10) in three patients with malignant hematologic disorders. Rinsho Ketsueki. 1992;33:1829-1833.
8. Pedersen-Bjergaard J, Timshel S, Andersen MK, Andersen AS, Philip P. Cytogenetically unrelated clones in therapy-related myelodysplasia and acute myeloid leukemia: experience from the Copenhagen series updated to 180 consecutive cases. Genes Chromosomes Cancer. 1998;23:337-349.
9. Andersen MK, Pedersen-Bjergaard J. Increased frequency of dicentric chromosomes in therapy-related MDS and AML compared to de novo disease is significantly related to previous treatment with alkylating agents and suggests a specific susceptibility to chromosome breakage at the centromere. Leukemia. 2000;14:105-111.
10. Greenberg P, Cox C, LeBeau MM, et al. International scoring system for evaluating prognosis in myelodysplastic syndromes. Blood. 1997;89:2079-2088.
11. Mauritzson N, Johansson B, Rylander L, et al. The prognostic impact of karyotypic subgroups in myelodysplastic syndromes is strongly modified by sex. Br J Haematol. 2001;113:347-356.
12. Alitalo T, Willard HF, de la Chapelle A. Determination of the breakpoints of 1;7 translocations in myelodysplastic syndrome by in situ hybridization using chromosome-specific alpha satellite DNA from human chromosomes 1 and 7. Cytogenet Cell Genet. 1989;50:49-53.
13. Kibbelaar RE, Mulder JW, van Kamp H, et al. Nonradioactive in situ hybridisation of the translocation t(1;7) in myeloid malignancies. Genes Chromosomes Cancer. 1992;4:128-134.
14. Fonseca R, Rajkumar SV, Ahmann GJ, et al. FISH demonstrates treatment-related chromosome damage in myeloid but not plasma cells in primary systemic amyloidosis. Leuk Lymphoma. 2000;39:391-395.
15. Seabright M. A rapid banding technique for human chromosomes. Lancet. 1971;2:971-972.
16. Yang Y, Kiss H, Kost-Alimova M, et al. A 1-Mb PAC contig spanning the common eliminated region 1 (CER1) in microcell hybrid-derived SCID tumors. Genomics. 1999;62:147-155.
17. Finelli P, Antonacci R, Marzella R, Lonoce A,

Archidiacono N, Rocchi M. Structural organization of multiple alphoid subsets coexisting on human chromosomes 1, 4, 5, 7, 9, 15, 18, and 19. Genomics. 1996;38:325-330.

18. Tapia-Paez I, Kost-Alimova M, Hu P, et al. The position of t(11;22)(q23;q11) constitutional translocation breakpoint is conserved among its carriers. Hum Genet. 2001;109:167-177.
19. Waye JS, England SB, Willard HF. Genomic organization of alpha satellite DNA on human chromosome 7: evidence for two distinct alphoid domains on a single chromosome. Mol Cell Biol. 1987;7:349-356.
20. Ogawa S, Toyoshima H, Kozutsumi H, et al. The C-terminal SH3 domain of the mouse c-Crk protein negatively regulates tyrosine-phosphorylation of Crk associated p130 in rat 3Y1 cells. Oncogene. 1994;9:1669-1678.
21. Lee C, Wevrick R, Fisher RB, Ferguson-Smith MA, Lin CC. Human centromeric DNAs. Hum Genet. 1997;100:291-304.
22. Willard HF. Centromeres: the missing link in the development of human artificial chromosomes. Curr Opin Genet Dev. 1998;8:219-225.
23. Jorgensen AL. Alphoid repetitive DNA in human chromosomes. Dan Med Bull. 1997;44:522-534.
24. Carine K, Jacquemin-Sablon A, Waltzer E, Mascarello J, Scheffler IE. Molecular characterization of human minichromosomes with centromere from chromosome 1 in human-hamster hybrid cells. Somat Cell Mol Genet. 1989;15:445-460.
25. Willard HF, Waye JS, Skolnick MH, Schwartz CE, Powers VE, England SB. Detection of restriction fragment length polymorphisms at the centromeres of human chromosomes by using chromosome-specific alpha satellite DNA probes: implications for development of centromere-based genetic linkage maps. Proc Natl Acad Sci U S A. 1986;83:5611-5615.
26. Wevrick R, Willard HF. Long-range organization of tandem arrays of alpha satellite DNA at the centromeres of human chromosomes: high-frequency array-length polymorphism and meiotic stability. Proc Natl Acad Sci U S A. 1989;86:9394-9398.
27. Alexandrov I, Kazakov A, Tumeneva I, Shepelev V, Yurov Y. Alpha-satellite DNA of primates: old and new families. Chromosoma. 2001;110:253-266.
28. Cooke HJ, Hindley J. Cloning of human satellite III DNA: different components are on different chromosomes. Nucleic Acids Res. 1979;6:3177-3197.
29. Tagarro I, Fernandez-Peralta AM, Gonzalez-Aguilera JJ. Chromosomal localization of human satellites 2 and 3 by a FISH method using oligonucleotides as probes. Hum Genet. 1994;93:383-388.
30. Wevrick R, Willard HF. Physical map of the centromeric region of human chromosome 7: relationship between two distinct alpha satellite arrays. Nucleic Acids Res. 1991;19:2295-2301.
31. Fetni R, Richer CL, Malfoy B, Dutrillaux B, Lemieux N. Cytologic characterization of two distinct alpha satellite DNA domains on human chromosome 7, using double-labeling hybridizations in fluorescence and electron microscopy on a melanoma cell line. Cancer Genet Cytogenet. 1997; 96:17-22.
32. Waye JS, Durfy SJ, Pinkel D, et al. Chromosome-specific alpha satellite DNA from human chromosome 1: hierarchical structure and genomic organization of a polymorphic domain spanning several hundred kilobase pairs of centromeric DNA. Genomics. 1987;1:43-51.
33. Schueler MG, Higgins AW, Rudd MK, Gustashaw K, Willard HF. Genomic and genetic definition of a functional human centromere. Science. 2001; 294:109-115.
34. Auriche C, Donini P, Ascenzioni F. Molecular and cytological analysis of a 5.5 Mb minichromosome. EMBO Rep. 2001;2:102-107.
35. Wevrick R, Willard VP, Willard HF. Structure of DNA near long tandem arrays of alpha satellite DNA at the centromere of human chromosome 7. Genomics. 1992;14:912-923.
36. Pedersen-Bjergaard J, Philip P, Larsen SO, et al. Therapy-related myelodysplasia and acute myeloid leukemia: cytogenetic characteristics of 115 consecutive cases and risk in seven cohorts of patients treated intensively for malignant diseases in the Copenhagen series. Leukemia. 1993;7:1975-1986.
37. Pedersen-Bjergaard J, Pedersen M, Roulston D, Philip P. Different genetic pathways in leukemogenesis for patients presenting with therapy-related myelodysplasia and therapy-related acute myeloid leukemia. Blood. 1995;86:3542-3552.

Leukemia (2003) 17, 1112–1120

www.nature.com/leu

Identification of a novel fusion gene, *TTL*, fused to *ETV6* in acute lymphoblastic leukemia with t(12;13)(p13;q14), and its implication in leukemogenesis

Y Qiao[1], S Ogawa[1], A Hangaishi[1], K Yuji[1], K Izutsu[1], A Kunisato[1], Y Imai[1], L Wang[1], N Hosoya[1], Y Nannya[1], Y Sato[2], K Maki[3], K Mitani[3] and H Hirai[1]

[1]*Department of Hematology and Oncology, Graduate School of Medicine, University of Tokyo, Tokyo, Japan;* [2]*Department of Clinical Pathology, Research Institute of Medicine Center of Japan, Tokyo, Japan; and* [3]*Department of Hematology, Dokkyo Medical College, Tokyo, Japan*

ETS variant gene 6 (*ETV6*)/translocation, ETS, leukemia (*TEL*)-involving chromosomal translocations are frequently observed in various hematologic neoplasms. We describe here a novel *ETV6*-involving translocation, t(12;13)(p13;q14), found in the case of acute lymphoblastic leukemia, in which *ETV6* fused with a previously unknown gene, named Twelve-thirteen Translocation Leukemia gene (*TTL*), at 13q14. *TTL* was weakly but ubiquitously expressed in normal human tissues as detected by reverse transcribed-PCR. Three *TTL* splicing forms were identified, *TTL-T* from a human testis cDNA library, with an open-reading frame of 402 bp encoding 133 amino acids (aa), and *TTL-B1* and *-B2* from a human brain cDNA library. These proteins have no homology to known proteins. In leukemic cells from the patient, both reciprocal fusion transcripts, *ETV6/TTL* and *TTL/ETV6*, were expressed. The predominant fusion transcript, *TTL/ETV6-1*, encodes a predicted 530 aa fusion protein containing 89 aa of the N-terminal *TTL* fusing to the helix–loop–helix domain and ETS-binding domain of *ETV6*. Although the function of *TTL* is yet to be elucidated, our findings will provide another insight into the molecular pathogenesis of leukemia having *ETV6*-involving translocations.

Leukemia (2003) **17,** 1112–1120. doi:10.1038/sj.leu.2402919
Keywords: chromosome translocation; leukemia; *ETV6/TEL*; *TTL*

Introduction

Leukemia-associated chromosomal translocations frequently result in the creation of aberrant fusion genes, which play a pivotal role in leukemogenesis.[1] A number of chimeric genes have been cloned and characterized from nonrandom translocations, including *AML1/MTG8* in t(8;21)(q22;q22),[2] *PML/RARA* in t(15;17)(q22,q21),[3] and *ETV6/PDGFRβ* in t(5;12)(q33;p13).[4] *ETV6* (ETS variant gene 6), also known as *TEL* (translocation, ETS, leukemia), is a member of the Ets family of transcription factors and is characterized by a C-terminal Ets domain responsible for specific DNA-binding activities and an N-terminal helix–loop–helix (HLH) oligomerization domain that is suggested to play a role in the protein–protein interaction with Ets factors to modulate transcriptional activity. *ETV6* is mapped to chromosome 12p13 and was originally identified as a gene that is fused to *PDGFRβ* gene in t(5;12)(q33;p13), one of the recurring chromosomal translocations found in chronic myelomonocytic leukemia (CMML).[4] Subsequently, a growing number of genes, including *ABL*,[5] *JAK2*,[6,7] *TRKC*,[8] *AML1*,[9–11] *MDS1/EVI1*,[12] *MN1*,[13] *CDX2*,[14] *STL*,[15] *BTL*,[16] *ARG*,[17] *ACS2*,[18] *HLXB9*,[19] and *PAX5*,[20] have been identified as fusion partners of *ETV6* in more than 40 different chromosomal translocations in a broad spectrum of hematopoietic neoplasms. In normal hematopoietic cells, *ETV6* appears to act as a transcriptional repressor and is essential for the definitive hematopoiesis.[21,22] However, several implications have been advanced as to the significance of functional modifications of *ETV6* and translocation partners in leukemogenesis. Therefore, the identification and characterization of new fusion partners of *ETV6* may help to further understand the critical role of *ETV6* in the development of leukemias with these *ETV6*-involving translocations.

t(12;13) is a rare, but recurring chromosome translocation described in a wide spectrum of leukemias including acute lymphoblastic leukemia (ALL),[23–27] AML,[28–34] CML,[35] CLL, and MDS.[30] A literature search revealed at least 35 or more cases with t(12;13) harboring breakpoints cytogenetically scattered from 12p11 to 12p13 and from 13q11 to 13q34. With regard to the breakpoints on 13q, there seem to exist at least three distinct types of translocations: t(12;13)(p11–13;q12), t(12;13)(p11–13;q14), and t(12;13)(p11–13;q34). Among them, 13 cases had a breakpoint at 12p13 and 13q14, including seven cases of ALL, four cases of AML, one CMML, and one MDS. In ALL, five had a pre-B-lineage phenotype and six were pediatric ALL. The molecular nature of these t(12;13)(p13;q14) translocations, however, has not been clarified to date.

We report here a molecular delineation of a case of t(12;13)(p13;q14) observed in an adult pre-B ALL, in which *ETV6* is rearranged with a novel gene, *TTL*, on 13q14, and both *ETV6/TTL* and *TTL/ETV6* fusion messages are transcribed. Our finding might provide important clues in understanding the molecular mechanism of the t(12;13)(p13;q14) translocation in leukemogenesis.

Materials and methods

Patients

The patient was a 46-year-old man, diagnosed as ALL in 1995. Cytogenetic analysis of his blasts showed a karyotype of 46,XY,add(6)(q15),t(12;13)(p13;q14),add(22)(q11). Once he attained a complete remission, but was relapsed thereafter and died of the refractory disease 4 years after the diagnosis. The immunophenotype of his blasts was CD10(+/−), CD19(+), CD20(−), CD33(+), and CD34(+). The sample used in this analysis was obtained with the informed consent.

Fluorescent in situ *hybridization (FISH)*

Since this translocation involves 12p13, which is the locus for *ETV6*, we investigated the potential involvement of *ETV6* gene by FISH experiments with a panel of cosmid probes containing different exons of *ETV6*. The cosmids were kindly provided by

Correspondence: Dr H Hirai, Department of Hematology and Oncology, Graduate School of Medicine, University of Tokyo, 7-3-1 Hongo, Bunkyo-ku, Tokyo 113-8655, Japan; E-mail: hhirai-tky@umin.ac.jp; Tel: 81-3-5800-6421; Fax: +81-3-5689-7286
Received 21 November 2002; accepted 3 February 2003

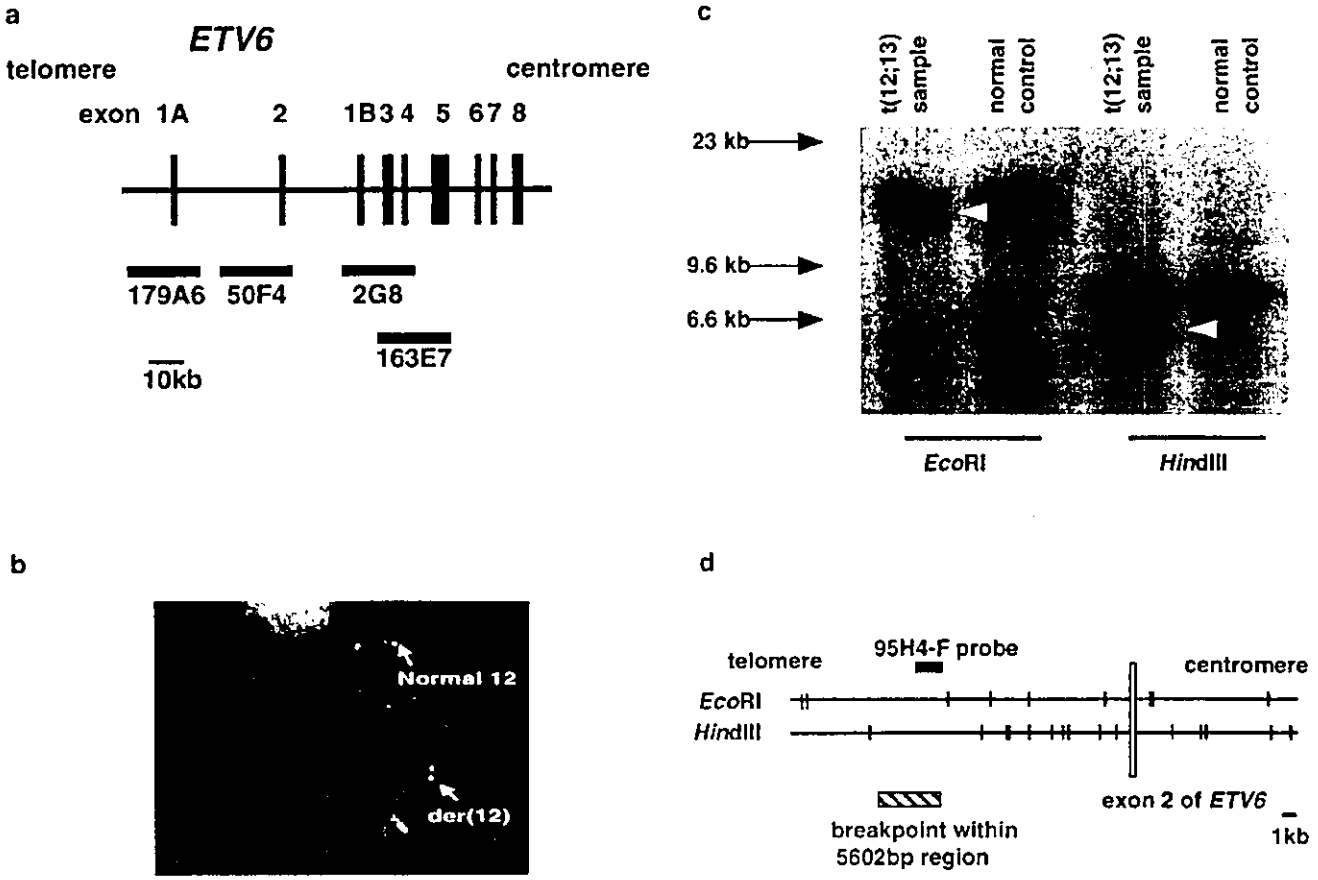

Figure 1 Analysis of breakpoint on chromosome 12. (a) A genomic map of *ETV6* exons and location of the cosmid probes used for FISH analysis. (b) FISH analysis of the patient's leukemic cells. The signals were found both on the der(12) and on the normal 12 with 2G8 probe, which contains exons 1B, 3 and 4. (c) Southern blot hybridization with a genomic probe (94H4-F). Rearranged bands, indicated by arrowheads, were found only in patient samples, but not in control cells. (d) A partial restriction map of cosmid 94H4 spanning the breakpoint region and *ETV6* exon 2. The location of the probe is indicated by a black box.

Dr Peter Marynen (University of Leuven, Belgium). The order and the relative locations of these cosmids are depicted in Figure 1a. FISH analyses on chromosome 12 were performed according to the standard procedures.[36,37] Briefly, the probes were labeled by nick translation using biotin-16-dUTP (Boehringer, Mannheim, Germany). After overnight hybridization and posthybridization washes, the hybridized probes were detected via an avidin–fluorescein isothiocyanate (Boehringer, Mannheim, Germany). For identification, chromosomes were counter stained with 4,6-diamidino-2-phenylinodole. The presence or absence of the FISH signals was scored on an average of three to six abnormal metaphase cells per probe.

Southern blotting

In all, 10 μg of high-molecular weight DNA were extracted from blood and bone marrow cells of this patient by standard procedure, digested to completion with either *Hin*dIII or *Eco*RI restriction endonucleases and subjected to Southern blot analysis as described.[38,39] According to the restriction enzyme map, a series of genomic probes covering the region from exons 1 to 3 of *ETV6* gene were prepared by genomic PCR and labeled with ^{32}P- deoxycytoxine triphosphate (dCTP) by random priming. PCR primers of 95H4-F1 and 95H4-R1 were used for making probe of 95H4-F.

Rapid amplification of cDNA end (RACE)

We adopted the RACE method to identify the fusion partners of *ETV6* in t(12;13)(p13;q14). Assuming both reciprocal fusion transcripts involving *ETV6*, 3'RACE was used for obtaining the 3' fusion fragment with *ETV6* exon 1, and 5'RACE for the 5' fusion fragment. Total RNA was extracted from a cryopreserved leukemic sample of this patient as described previously.[38] For 3'RACE, the primer R2N6 was used for reverse transcription.[7] Nested 3'RACE-PCR was performed using primers specific for *ETV6* exon 1, *ETV6*-F1a and *ETV6*-F1b, in combination with primers N6R1 and N6R2, respectively.[7,16] For 5'RACE, the first-strand cDNA was tailed with dCTP, followed by nested PCR with primers specific for *ETV6* exon 3, *ETV6*-R3a and *ETV6*-R3b,[16] in combination with primers of 5'-adaptor-UAP-1 and 5'-adaptor-UAP-2, respectively. The nucleotide sequences of primers R2N6, N6R1, N6R2, *ETV6*-F1a, *ETV6*-F1b, *ETV6*-R3a, and *ETV6*-R3b are the same as described by Peeters *et al*[7] and Cools *et al*.[16] The thermal cycling profile was as follows: 94°C for 2 min followed by 35 cycles of 94°C for 45 s, 60°C for 45 s, 72°C for 90 s, and a final extension at 72°C for 10 min. The PCR products were subcloned into the TA vector (Invitrogen, Tokyo, Japan) and the positive colonies were screened by colony hybridization using the standard protocols. We isolated clones positive for the *ETV6* exon 1 but negative for *ETV6* exon 2 in the 3'RACE experiment, and those positive for *ETV6* exon 2 and

negative for *ETV6* exon 1 in the 5'RACE experiment were selected. All the selected clones were sequenced using fluorescently labeled dideoxy terminators on the 377 Applied Bisystems automated sequencer (Applied Biosystems, Urayasu, Japan).

cDNA library screening

Human testis and brain cDNA libraries in lambda gt11 (10^9 pfu/ml) (kindly provided by Dr Shuntaro Ikawa, Tohoku University, Japan) were screened for cDNAs of the fusion partner with the fragments identified by 3'RACE experiments as probes. The probes were labeled with ^{32}P-dCTP by random priming. Positive clones were subcloned into pBluescript-KS(−) and sequenced.

Radiation hybrid mapping

The GeneBridge 4 Radiation Hybrid Panel (Research Genetics, Huntsville, AL, USA) was used for chromosome mapping. A series of PCRs were carried out for this panel by using primers RHM-F and RHM-R, which are specific for the fragments identified by 3'RACE experiments. The PCR cycle condition was as follows: one initial cycle of 2-min denaturation at 94°C, followed by 45 cycles of 30-s denaturation at 94°C, 30-s annealing at 60°C and 1-min extension at 72°C, and a final cycle extension of 10-min at 72°C. The PCR results from the radiation mapping vectors were formatted according to the manufacturer's instructions and were analyzed using the server at the Stanford Human Genome Center (http://www-shgc.stanford.edu) to search the STS markers on the screening panel.

Reverse transcribed reaction-PCR (RT-PCR)

In all, 5 μg of the total RNA from leukemic cells of the patient were RT with 2 U of Moloney murine leukemia virus reverse transcriptase (MMLV-RT, Stratagene, USA) using a random hexamer or an oligo-dT primer (Ro-Ri-oligo-dT).[14] One tenth of the synthesized cDNA was directed to PCR analysis. For amplification of *ETV6/TTL* transcripts, primers *ETV6*-F1 and *TTL*-R1 were used for the first round, and *ETV6*-F2 and *TTL*-R2 for the second round. The first and second round primers for *TTL/ETV6* were *TTL*-F1 and *ETV6*-R1, and *TTL*-F2 and *ETV6*-R2, respectively (Figure 2). For amplification of *TTL* messages, we used *TTL*-F3 and *TTL*-R3 for the first round PCR, and *TTL*-F4 and *TTL*-R4 for the second round. For detection of full-length *ETV6* expression from leukemic cells of the patient, primers *ETV6*-F1 and *ETV6*-R3 were used in the RT-PCR. The PCR conditions were the same as described above.

Quantitative real-time RT-PCR

Quantitative real-time RT-PCR was performed using a LightCycler-FastStart DNA Master SYBR Green I kit and instrument (Roche Diagnostics, Mannheim, Germany). For the construction of standard curves, *ETV6*- and *TTL/ETV6*-containing plasmids, pME18s-*ETV6* and pME18s-*TTL/ETV6*,[40] were used with serial dilutions according to the manufacturer's instructions and the concentration of $MgCl_2$ was adjusted to 2 mM. The RT cDNA samples from the patient were prepared as described above. PCR primers for *ETV6* amplification are *ETV6*-F3 and *ETV6*-R4, and those for *TTL/ETV6* are *TTL*-F4 and *ETV6*-R2. PCR conditions are as follows: initial denaturation at 95°C for 10 min, followed by 30 cycles at 95°C for 15 s, 60°C for 5 s and 72°C for 8 s. Data were calculated by using LightCycler™ analysis software provided by the LightCycler apparatus. The specificity of the PCR reactions was also verified by ethidium bromide staining on 2% agarose gels.

Primers

Primers used in PCRs were listed in the Table 1.

Results

Identification of the breakpoint on chromosome 12

From the G-banding analysis, the breakpoint on chromosome 12 was expected to be within *ETV6* gene. To test this, we performed FISH experiments using several probes from the *ETV6* locus (Figure 1a). Hybridization signals from cosmids 179A6 and 50F4, which contain exons 1A and 2 of *ETV6* gene, respectively, were found on der(13) as well as the apparently normal chromosome 12 (data not shown), whereas signals from cosmids 2G8 (Figure 1b) and 163E7 (data not shown) containing exons 1B, 3–5 , respectively, were on der(12) but not on der(13), indicating the breakpoint on 12p13 to be within *ETV6* gene, around exon 2. To further define the breakpoint on 12p13, Southern blot was performed with a series of genomic probes covering the range of introns 1 and 2 of *ETV6* gene. With a genomic probe located in the intron 1 of *ETV6* gene, tumor-specific rearrangement bands were identified (Figure 1c and d). According to the restriction map of *ETV6* and the sequence analysis of the locus, the breakpoint on 12p13 was finally localized within a 5.6 kb *Hin*dIII/*Eco*RI fragment, which is between *ETV6* exons 1 and 2, (Figure 1d), indicating a possibility that *ETV6* may participate in the genetic aberration that would result in the generation of a fusion transcript involving the other yet undefined gene on 13q14.

Identification of the fusion partner of ETV6 *with RACE-PCR*

To identify the possible fusion partner of *ETV6*, we tried 3' as well as 5'RACE-PCRs for leukemic samples from the patient. Although the 5'RACE PCR failed to amplify possible fusion messages, 3'RACE-PCR products were successfully obtained, subcloned into plasmids, and screened by colony hybridization, in which colonies positive for *ETV6* exon 1 and negative for *ETV6* exon 2 were isolated and subjected to the sequencing analysis. All the analyzed clones contain a still unknown sequence with a consensus 450 bp in length (F450 fragment in Figure 2a) immediately after the end of the *ETV6* exon 1. As shown below, the latter unknown sequence was revealed to be a part of a novel gene, designated as *TTL* for Twelve-thirteen Translocation Leukemia gene. The chimeric transcript comprises the *ETV6* exon 1 in-framely fusing to the F450 fragment, within which a stop codon appears 60 bp downstream from the fusion point. To further confirm the localization of the F450 fragment, we performed radiation hybrid mapping. The data were transmitted and analyzed by the Stanford Human Genome Center and indicated that this novel sequence was

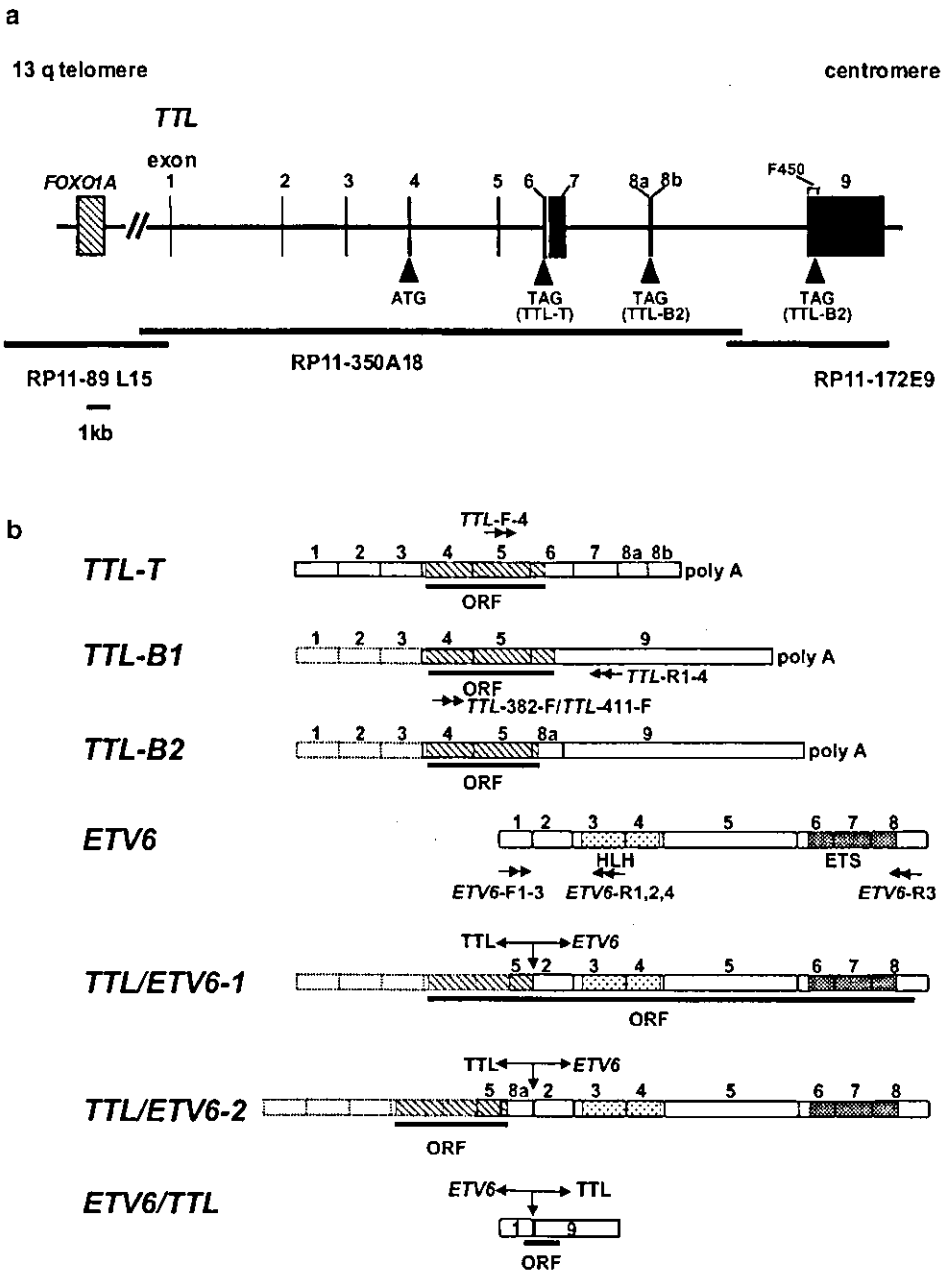

Figure 2 Schematic diagrams of *TTL* and its fusions with *ETV6*. (a) Genomic organization of *TTL* exons (black boxes) and *FOXO1A* gene (a hatched box) are illustrated with corresponding BAC clones. The locations of putative initiation and stop codons are indicated by arrowheads. (b) Schematic representations of three alternative splicing forms of *TTL*, *ETV6*, and the fusion transcripts. The expected ORF of each transcript is underlined with solid bars. The ORFs of different *TTL* splicing forms are also shown by hatched boxes. Boxes with broken border indicate possible sequences that could not be successfully isolated but expected to be present in each splicing form. Double arrows are the positions of RT-PCR primers as described in the materials and methods. HLH: helix–loop–helix domain, ETS: Ets-family DNA-binding domain.

located on the long arm of chromosome 13, between CHLC.GATA6B07 and WI-13180.

Identification of full-length cDNAs for a novel gene, TTL

Since the unknown 450 bp sequence from the putative novel gene, *TTL*, has no homology to known genes, we first examined its expression in human tissues. Northern blot analysis using a human RNA panel failed to detect any *TTL* transcripts. However, using nested RT-PCR, we could find almost ubiquitous *TTL* expression in human tissues, including lung, liver, thymus, and bone marrow (Figure 3a). The *TTL* message could be detected on the first round of the nested PCR in brain and testis, suggesting relatively higher expression of *TTL* in these tissues. By screening human testis and brain cDNA libraries with the 450 bp novel sequence (F450 fragment) as a probe and employing 5′ and 3′RACE and RT-PCR, we identified three splicing forms of *TTL*, *TTL-T*, *TTL-B1* and *-B2* (Figures 2b and 4. Accession nos. AY116214, AY116215, and AY116216,

Table 1 Primers used for PCR amplifications

Name	*Sequence (5′→3′)*
94H4-F1	GCCGGTGTTGCTATTACTCC
94H4-R1	CTTTGGGACACATGCCATAA
5′-adaptor-UAP-1	CCAGTGAGCAGAGTGACGAGGAC TCGAGCTCAAGCGGGGGGGG
5′-adaptor-UAP-2	CCAGTGAGCAGAGTGACG
RHM-F	AACAGCATGGAGCAAGGAAA
RHM-R	GGAGAGACTGACCCATGGAC
ETV6-F1	TCCTGATCTCTCTCGCTGTG
TTL-R1	TTTCCTTGCTCCATGCTGTT
ETV6-F2	GAGACTCCTGCTCAGTGTAGC
TTL-R2	CACCTGAGTCCTCAGAAAAGC
TTL-F1	CATTGCTGAGATGAGTGAGGA
ETV6-R1	GTGTTGCTGTCAATTGGCCT
TTL-F2	TCAGAAAATCAGGCCTCCTC
ETV6-R2	GAAAACTCATTTTCAGCCCAC
TTL-F3	TCAGAAAATCAGGCCTCCTC
TTL-R3	CAGACTGGCCAACAGAGACA
TTL-F4	GGAATGTGCCTCAGCTTCTG
TTL-R4	GTGTGAGGAGAGGGGTCAAA
ETV6-R3	AAGTGTCCCTGCCATTTCTG
ETV6-F3	TGAGACATGTCTGAGACTCCTGCT
ETV6-R4	TCGAGTCTTCCTCCATCCTG
TTL-382-F	CCTGGAACATGGAAGATGCT
TTL-411-F	TTTGCTGAAGGAACGAGTGA

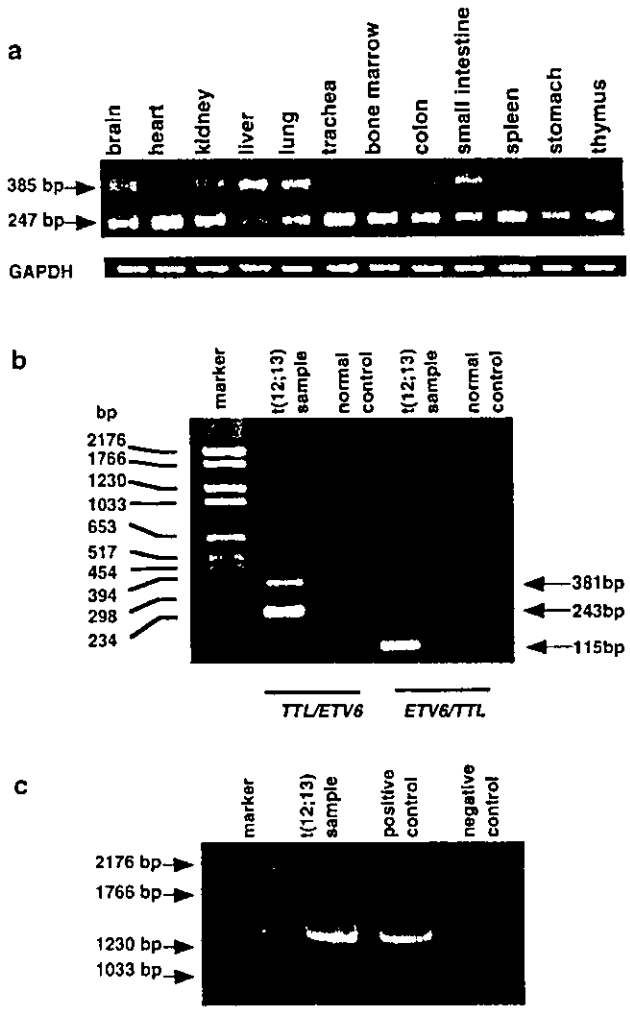

Figure 3 Expression of *TTL* and *TTL* fusion transcripts. (a) RT-PCR analysis of *TTL* expression in normal human tissues. Two specific bands were detected according to the presence or absence of the exon 8a in the transcripts as revealed by sequencing of the PCR products. Primers, *TTL*-F3 and *TTL*-R3, were for the first round PCR, and *TTL*-F4 and *TTL*-R4 for the second round PCR. GAPDH positive controls are shown below. (b) Detection of *TTL/ETV6* as well as *ETV6/TTL* fusion messages by RT-PCR in the patient's leukemic sample. Two alternative forms of *TTL/ETV6* (with primers *TTL*-F1 and *ETV6*-R1 for the first round PCR and *TTL*-F2 and *ETV6*-R2 for the second round) and a single *ETV6/TTL* fusion transcript (with primers *ETV6*-F1 and *TTL*-R1, and *ETV6*-F2 and *TTL*-R2 for the first and second round PCR, respectively) are specifically detected in leukemic cells having t(12;13)(p13;q14). (c) Detection of *ETV6* message with RT-PCR. With primers within *ETV6* exon 1 (*ETV6*-F1 primer) and exon 8, (*ETV6*-R3 primer) the predicted product is 1516 bp in length.

respectively.) The sequences of these clones were further used to search GeneBank for genomic clones corresponding to the *TTL* locus, and we identified two BAC clones for the *TTL* locus, namely, clone RP11-350A18 and clone RP11-172E9 (Figure 2a). By comparing cDNA sequences with deposited genomic sequences of these clones, we determined the genomic organization of *TTL* exons depicted in Figure 2.

TTL-T, isolated from human testis library, is 2090 bp in length with a polyA tail and composed of *TTL* exons 1–8. The longest open-reading frame (ORF) of *TTL-T*, that follows the Kozac's rule, harbors exons 4, 5, and a part of exon 6, encoding 133 amino acids (aa) which so far has no homology to known proteins in GeneBank (Figures 2a and 4a).

TTL-B1 on the other hand, was originally isolated from the human brain library as a fragment containing part of exons 5 and 9. By 3′RACE in combination with a series of PCR experiments (data not shown), we determined its polyA end that appeared at the terminal of exon 9 consisting of 3183 bp. In the following nested RT-PCR on human testis RNA using outer (*TTL*-382-F, *TTL*-R3) and inner (*TTL*-411-F, *TTL*-R4) primary sets (Figure 2b), we identified a transcript that contained *TTL* exons 4, 5, and a 5′ sequence of exon 9. Thus, the expected *TTL-B1* splicing form consists of at least 3450 bp and contains an ORF, which starts from the same start codon as *TTL-T* but differentially terminates at the 20th codon (TGA) of exon 9 (Figures 2b and 4b).

Finally, we also found the other form of *TTL*, *TTL-B2*, in which the exon 8a sequence is inserted between exons 5 and 9. Expression of this form of transcript was detected by RT-PCR in a wide variety of tissues and cell types, including bone marrow, thymus, spleen, and liver (Figure 3a, the large band). Although we could not isolate the full length of *TTL-B2*, it may well correspond to the *TTL-B1* form with an exception that it has the insertion of exon 8a between exons 5 and 9 (Figures 2b and 4b). The putative *TTL-B2* has 3588 bp and its ORF is supposed to share the same ATG codon with *TTL-B1* and *TTL-T*, but stopped immediately within exon 8a (Figures 2b and 4b). Thus, the predicted amino acids from the three splicing form share the first 89 aa encoded by a part of exons 4 and 5, but have different carboxyl termini depending on the different splicing.

Expressions of *TTL-B1*, *TTL-B2* (Figure 3a), and *TTL-T* (data not shown) were demonstrated by nested RT-PCR in a variety of normal tissues (Figure 3a) as well as leukemia/lymphoma cell lines, including Raji (B-malignant lymphoma), HPB-NULL (B-ALL), BALM1 (B-ALL), KCL22 (B-CML), MT1 (T-ATL), Peer (T-ALL), ATL35 (T-ATL), and Jurkat (T-ALL) (data not shown).

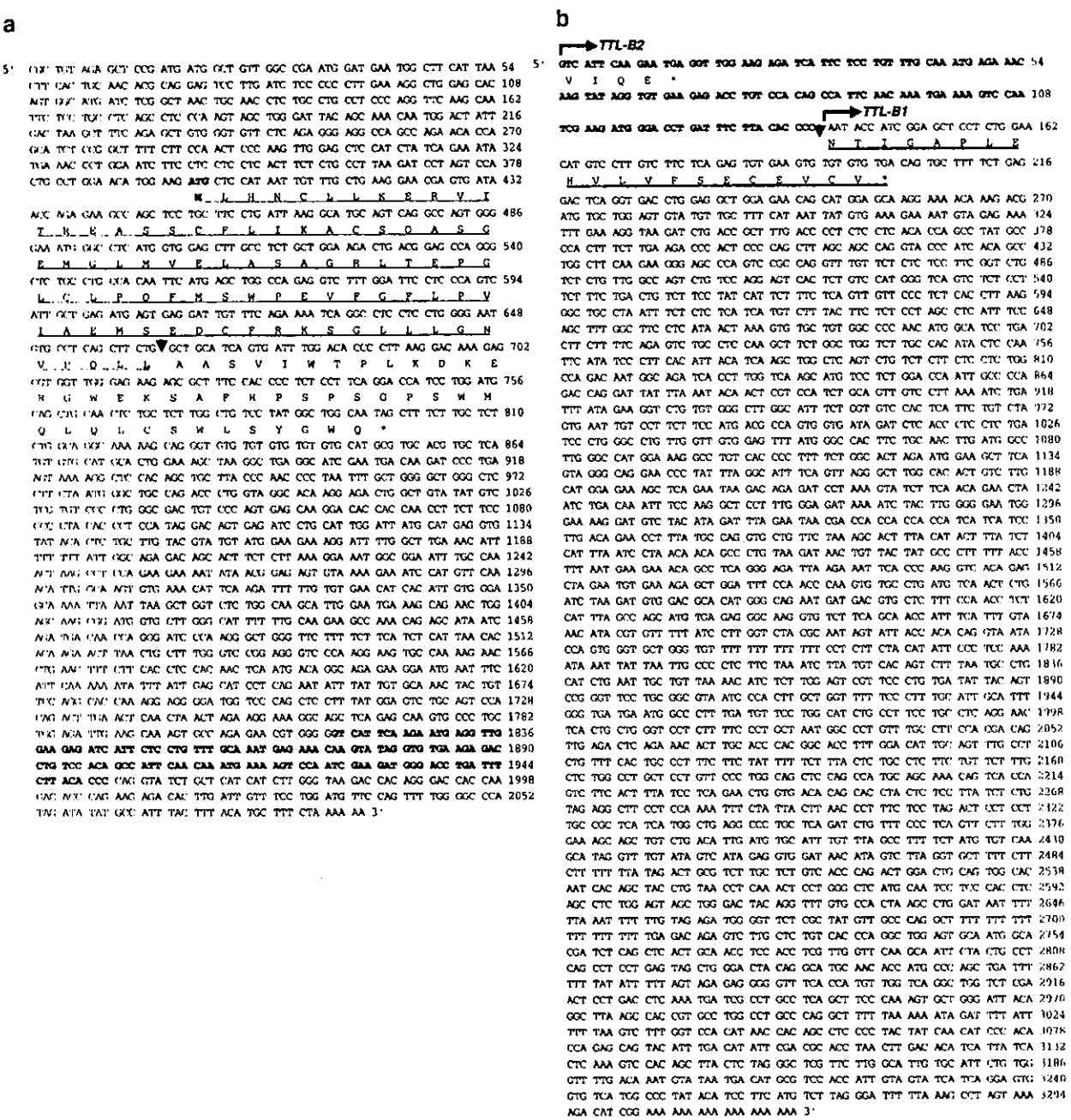

Figure 4 cDNA and predicted amino-acid sequences of *TTL*. (a) *TTL-T* sequence. The ATG coden is shown by bold italic. The asterisk (*) indicates a stop codon. The singly underlined 89 aa encoded by exons 4 and 5 are shared in common by all three *TTL* splicing forms. (b) Partial cDNA sequence of *TTL-B1* and *TTL-B2* following the commonly shared exons 4 and 5. Exon 8a, as shown by bold in both (a) and (b), is inserted between exons 4 and 9 in *TTL-B2*, but not in *TTL-B1*. *TTL-B1* and *TTL-B2* are supposed to share the same ATG codon as *TTL-T* in (a). The ORF of *TTL-B1* consists of the singly underlined 89 aa in (a) and the doubly underlined 20 aa in (b), while the *TTL-B2* ORF is composed of the singly underlined 89 aa in (a) and the 4 aa acids encoding first 12 bp of exon 8a. The asterisk indicates a stop codon. The breakpoint is shown by an arrowhead.

Detection of the TTL/ETV6 *and* ETV6/TTL *fusion transcripts with nested RT-PCR*

Both reciprocal fusion transcripts, *TTL/ETV6* and *ETV6/TTL*, were detected in the primary tumor sample by nested RT-PCR (Figure 3b). To identify the *TTL/ETV6* fusion, nested RT-PCR analysis on patient materials was performed using forward primers in *TTL* exon 5, and reverse primers in *ETV6* exon 3. As shown in Figure 3b, two bands were specifically amplified from the sample of the patient. Sequence analysis disclosed that the smaller but major band (*TTL/ETV6-1*) corresponded to the in-frame fusion of part of the exon 5 of *TTL* to the 5′ end of *ETV6* exon 2, while the larger one (*TTL/ETV6-2*) was an out-of-frame fusion of the part of exons 5 and 8a of *TTL* to the *ETV6* exon 2

(Figure 2b). The ORF of the latter fusion transcript is prematurely terminated in the stop codon within exon 8a of *TTL* before it fuses to *ETV6* exons. The reciprocal chimeric transcript of *ETV6* exon 1 and *TTL* (*ETV6/TTL*) could also be detected by RT-PCR, in which *ETV6* exon 1 was fused to the 5′ end of the exon 9 of *TTL-B* (Figure 2b). We evaluated the integrity of the remaining *ETV6* locus by FISH analysis, in which all the signals of the four cosmid probes were normally detected on the remaining, apparently normal chromosome 12, indicating that the other *ETV6* locus is grossly intact with no large deletions. To confirm the expression of *ETV6* from the intact allele, we performed RT-PCR analysis for the patient's leukemic sample using primers located within *ETV6* exons 1 and 8. As shown in Figure 3c, the leukemic sample clearly showed *ETV6* expression. Sequencing analysis of the RT-PCR product confirmed that there were no mutations in the RT product.

Analysis of mRNA expression levels of ETV6 *and* TTL/ETV6

We measured expression levels of *ETV6* and *TTL/ETV6* transcripts in the leukemic cells of the patient by the quantitative real-time RT-PCR analysis using LightCycler™. It demonstrated that the level of *TTL/ETV6* transcript was 40-fold lower than that of *ETV6* transcript (Figure 5a). Agarose gel analysis showed RT-PCR bands of the correct size (Figure 5b).

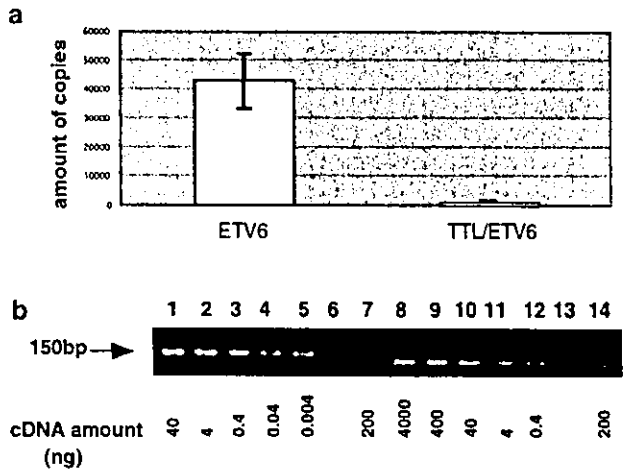

Figure 5 Real-time quantitative RT-PCR analysis of *ETV6* and *TTL/ETV6* transcripts in patient's leukemic sample. (a) Normalized expression of *ETV6* and *TTL/ETV6* using the LightCycler™ system. Each assay was performed in duplicate. (b) Agarose gel electrophoresis of real-time RT-PCR products of *ETV6* (lanes 1–7) and *TTL/ETV6* (lanes 8–14). Two plasmid constructs, pME18s/*ETV6* (lanes 1–5) and pME18s-*TTL/ETV6* (lanes 8–12), were used as standards with 10-fold serial dilutions starting from 40 ng/tube and 4 μg/tube for quantification of *ETV6* and *TTL/ETV6* messages in patient's samples, respectively. Lanes 6 and 13 are negative controls. 200 ng (lanes 7 and 14) of cDNA from the leukemic sample were subjected to the real-time PCR assay.

Discussion

t(12;13)(p13;q14) is a recurring reciprocal chromosome translocation found in ALL as well as in AML, CML, CLL, and MDS. From the cytogenetic analysis, it is thought to be cytogenetically distinct from t(12;13)(p13;q12), in which *ETV6* is shown to be combined with *CDX2*.[14] In fact, the *ETV6/CDX2* message was not detected by RT-PCR in our case (data not shown). Rather we have revealed that a novel gene, *TTL*, at 13q14 was rearranged with *ETV6* at 12p13, resulting in reciprocal fusion transcripts, *TTL/ETV6* and *ETV6/TTL*, in a case with t(12;13)(p13;q14). However, it is still unclear whether all the cases described as t(12;13)(p13;q14) have the same molecular abnormality, since they have been reported to involve leukemias of apparently different lineages.

The involvement of the *ETV6* gene in leukemia-associated translocations is notable for its wide variety of fusion partners with different breakpoints in various subtypes of leukemias.[41] This promiscuous feature of *ETV6*-involving translocations and their breakpoint variations apparently make it difficult to give a simplified and straightforward explanation for the leukemogenic mechanism of *ETV6*-involving translocations. Rather, it seems to involve different modalities according to the context of the type of translocations.

Clearly, the functional modification of the fusion partners is critically important in some cases. For examples, in *ETV6/PDGFRβ* and other fusions involving *ETV6* and tyrosine kinases, the HLH domain of *ETV6* functions as a homodimerization motif that is necessary for the constitutive activation of their C-terminal tyrosine kinases.[42] In t(12;21), the *ETV6/AML1* inhibits the function of *AML1* in a dominant-negative fashion.[43] In other cases, in contrast, there are no known functional domains of *ETV6* or the partner proteins found in the fusion products (such as *ETV6/STL*[15] or *ETV6/BTL*[16]), or only a tiny garbage sequence derived from the partner followed by one or more functional domains of *ETV6* (such as *HLXB9/ETV6*,[19] *ACS2/ETV6*,[18] and *PAX5/ETV6*[20]) or *vice versa* (*ETV6/CDX2*[14] and *ETV6/MDS1/EVI1*[12]). In the latter examples, the promoter of *ETV6* might drive ectopic expression of the transcription factors, *CDX2* and *EVI1*.

In the current translocation, both possible reciprocal fusion transcripts, *TTL/ETV6* and *ETV6/TTL*, were expressed in the tumor cells, which is also the case with *MN1/ETV6* and *ETV6/MN1* in t(12;22)(p13;q11),[13] *ACS2/ETV6* and *ETV6/ACS* in t(5;12)(q31;p13),[18] and *STL/ETV6* and *ETV6/STL* in t(6;12)(q23;p13).[15] With regard to *ETV6/TTL* fusion transcript, the 3′*TTL* sequence introduced an in-frame stop codon 60 bp after the end of *ETV6* exon 1, resulting in only a potential 31 aa, and it could be hardly expected that this extremely short fusion protein would have any functional roles. The other transcript, *TTL/ETV6*, has two splicing forms, the predominant *TTL/ETV6-1* and less abundant *TTL/ETV6-2*. The predominant *TTL/ETV6-1* transcript was a direct in-frame fusion between *TTL* exon 5 and *ETV6* exon 2, in which the first 11 aa of *ETV6* are replaced by 89 aa from the potential ORF of *TTL*. Since the predicted 530-aa fusion protein consists mostly of *ETV6* with both HLH and ETS domains being preserved, it might potentially have some transcriptional activities, most likely to modify *ETV6* function. However, in quantitative estimation using real-time PCR, the expression of *TTL/ETV6* was almost negligible compared with the remaining expression of *ETV6*, and we could not attribute any functional significance to this fusion protein.

In view of no functional implications in the resulting fusion proteins, the pathological significance of this translocation would be better explained by the hypothesis of loss of function of *ETV6* and/or *TTL*. It has been much discussed that loss of, and even haplo-insufficiency of *ETV6* function might be important for leukemogenesis, based on the observation that the second *ETV6* allele is deleted in some *ETV6* translocations, especially in more than 90% of cases associated with t(12;21).[44,45] *In vitro*